








# Dosage sensitivity to Pumilio1 variants in the mouse brain reflects distinct molecular mechanisms

Salvatore Botta<sup>1,2</sup> , Nicola de Prisco<sup>1</sup>, Alexei Chemiakine<sup>1</sup> , Vicky Brandt<sup>1</sup>, Maximilian Cabaj<sup>1</sup>, Purvi Patel<sup>3</sup> , Ella Doron-Mandel<sup>4</sup>, Colton J Treadway<sup>5</sup> , Marko Jovanovic<sup>4</sup>, Nicholas G Brown<sup>5</sup> , Rajesh K Soni<sup>3</sup>  & Vincenzo A Gennarino<sup>1,6,7,8,\*</sup> 

## Abstract

Different mutations in the RNA-binding protein Pumilio1 (PUM1) cause divergent phenotypes whose severity tracks with dosage: a mutation that reduces PUM1 levels by 25% causes late-onset ataxia, whereas haploinsufficiency causes developmental delay and seizures. Yet PUM1 targets are derepressed to equal degrees in both cases, and the more severe mutation does not hinder PUM1's RNA-binding ability. We therefore considered the possibility that the severe mutation might disrupt PUM1 interactions, and identified PUM1 interactors in the murine brain. We find that mild PUM1 loss derepresses PUM1-specific targets, but the severe mutation disrupts interactions with several RNA-binding proteins and the regulation of their targets. In patient-derived cell lines, restoring PUM1 levels restores these interactors and their targets to normal levels. Our results demonstrate that dosage sensitivity does not always signify a linear relationship with protein abundance but can involve distinct mechanisms. We propose that to understand the functions of RNA-binding proteins in a physiological context will require studying their interactions as well as their targets.

**Keywords** AGO2; brain interactome; FMRP; RBP interactome; RNA-binding protein interactome

**Subject Categories** Neuroscience; RNA Biology

**DOI** 10.15252/embj.2022112721 | Received 29 September 2022 | Revised 1 March 2023 | Accepted 14 March 2023 | Published online 18 April 2023

**The EMBO Journal (2023) 42: e112721**

## Introduction

RNA-binding proteins (RBPs) modify the proteome at the posttranscriptional level, regulating RNA localization, transport, translation, splicing, and decay; they have been found to orchestrate hundreds of pathways that are responsible for proper biological functions (Keene, 2007b; Hentze *et al.*, 2018). As our understanding of RBPs has grown over the past decade, it has become clear that their functions are particularly important in neurons, whose synaptic plasticity demands rapid local responses to stimuli (Mauger *et al.*, 2016). Several complex neurological disorders—for example, Fragile X syndrome, Fragile X-associated tremor and ataxia syndrome, and amyotrophic lateral sclerosis—are known to involve disruptions in the function of RBPs, which has understandably led to considerable interest in mapping their neuronal targets (Darnell & Richter, 2012; Khalil *et al.*, 2018; Ravanidis *et al.*, 2018).

Targets may not provide a full picture of the RBP's activities, however. Several years ago, we had discovered that the RBP Pumilio1 (Pum1) is important for mouse neurobiology (Gennarino *et al.*, 2015), which prompted us to search for human patients bearing mutations in PUM1. (As we will refer to both mouse and human proteins and genes in this paper, we will capitalize only the latter.) We initially identified 15 individuals with various degrees of loss of function, whose phenotypic severity tracked with protein dosage. The mildest variant (T1035S), which reduces PUM1 levels by only 25%, causes a slowly progressive, pure ataxia with onset in the later decades of life, whereas the most severe missense mutation (R1147W) reduces PUM1 levels by ~50% and causes a severe developmental syndrome. (Both the infantile and adult-onset phenotypes are now considered to be forms of spinocerebellar ataxia type 47 [SCA47, MIM: 617931], but in this work we will refer to the adult

1 Department of Genetics and Development, Columbia University Irving Medical Center, New York, NY, USA

2 Department of Translational Medical Science, University of Campania Luigi Vanvitelli, Caserta, Italy

3 Proteomics and Macromolecular Crystallography Shared Resource, Herbert Irving Comprehensive Cancer Center, Columbia University Irving Medical Center, New York, NY, USA

4 Department of Biological Sciences, Columbia University, New York, NY, USA

5 Department of Pharmacology and Lineberger Comprehensive Cancer Center, University of North Carolina School of Medicine, Chapel Hill, NC, USA

6 Departments of Neurology, Columbia University Irving Medical Center, New York, NY, USA

7 Columbia Stem Cell Initiative, Columbia University Irving Medical Center, New York, NY, USA

8 Initiative for Columbia Ataxia and Tremor, Columbia University Irving Medical Center, New York, NY, USA

\*Corresponding author. Tel: +1 212 305 7863; E-mail: vag2138@cumc.columbia.edu

disease as PUM1-related cerebellar ataxia [PRCA] and the neurodevelopmental syndrome as PUM1-associated developmental delay and seizures [PADDAS]; Gennarino *et al*, 2018.) T1035S lies within a highly conserved RNA-binding domain and therefore impairs RNA binding, so it was not surprising to find known PUM1 targets upregulated in patient cells—but R1147W, which lies outside this domain and does not impair target regulation, upregulated the same targets to the same degree (Gennarino *et al*, 2018). Moreover, the R1147W phenotype is quite severe, closer to that of the null mice than the heterozygous mice. It therefore seems that target dysregulation might not account for the effects of R1147W. Given that RBPs can interact with, influence, or compete with each other (Dassi, 2017), we hypothesized that R1147W might disrupt PUM1's ability to interact with its native partners, which would then lead to derepression of the targets of these complexes and not just the direct targets of PUM1.

To test this hypothesis requires, first, that we identify Pum1 interactors in the mouse brain, which is not a trivial undertaking. Protein interactions in general, and those of PUF (Pumilio and FBF) family members in particular, can be organism-, transcript-, tissue-, and even condition-specific (Marrero *et al*, 2011). Pumilio was discovered over 20 years ago to serve crucial roles in germline stem cell maintenance and embryogenesis in *Drosophila* and *C. elegans* (Wickens *et al*, 2002), and studies of its targets reveal it to be involved in development, host defense, and response to stressors in yeast and plants (Wickens *et al*, 2002; Miles *et al*, 2012; Goldstrohm *et al*, 2018; Uyhazi *et al*, 2020; Huh, 2021). Almost nothing is known about Pum1 function in the mammalian brain, however, beyond embryonic neurogenesis (Zhang *et al*, 2017). We therefore took an unbiased approach by using *in vivo* proteomics to identify PUM1's native partners in the mouse brain. We then studied the effect of Pum1 insufficiency on a subset of interactors in *Pum1* heterozygous and null mice and cell lines from patients bearing either the T1035S or R1147W mutation, followed by *in vitro* experiments with purified, tagged proteins.

## Results

### Establishing the PUM1 interactome in the adult mouse brain

We performed co-immunoprecipitation (IP) on brains from 10-week-old wild-type (WT) mice followed by liquid chromatography with tandem mass spectrometry (LC–MS/MS); we used IgG as a negative control (Appendix Fig S1A). Principal component analysis (PCA) separated IP-IgG from IP-Pum1 (Appendix Fig S1B). No residual Pum1 was detected in the brain tissue by post-IP western blot (Appendix Fig S1C). (In this paper, we will differentiate between human and mouse proteins by using all-caps only for the former.) Considering only those candidates that had at least two unique peptides in at least five out of six IP-Pum1 samples, this approach identified 234 putative interactors (Dataset EV1) that we clustered into 10 functional groups using protein–protein interaction data from CORUM and the Human Protein Atlas (Raudvere *et al*, 2019; Fig 1).

Our list included several proteins that had been previously found to interact with Pum1, as well as new members of protein complexes or families that interact with Pum1 in other contexts. For example, our

LC–MS/MS identified Fmrp (in cluster 7), which associates with Pum1 in neural progenitor cells (Zhang *et al*, 2017). We also identified Cnot1, the central scaffold of the CCR4–NOT complex (Van Etten *et al*, 2012; Enwerem *et al*, 2021), which is recruited by Pum1 to shorten poly(A) tails and promote mRNA degradation (Van Etten *et al*, 2012; Temme *et al*, 2014; Weidmann *et al*, 2014). Translation initiation factors (cluster 6) were previously found to cooperate with PUF proteins in invertebrates (Blewett & Goldstrohm, 2012).

*Drosophila* studies showed that Pumilio interacts with different proteins in different neuronal types (Muraro *et al*, 2008), so we repeated the LC–MS/MS experiments in the cerebellum, hippocampus, and cortex, three brain regions that abundantly express Pum1 (Gennarino *et al*, 2015). PCA readily separated Pum1 and IgG samples (Appendix Fig S2A–D). This analysis identified 854 putative Pum1 interactors in the cerebellum, 422 in the hippocampus, and 598 in the cortex (Fig 2A, and Dataset EV1); 489 were unique to the cerebellum, 145 to the hippocampus, 247 to the cortex, and 48 to the rest of the brain (i.e., excluding these three regions). Only 82 candidates appeared in all three brain regions and the whole brain (Fig 2A, yellow dots).

To ensure that these results do not merely reflect regional differences in protein abundance, we performed quantitative proteomics in 10-week-old whole brain, cerebellum, cortex, and hippocampus. In general, Pum1 interactors were not the most abundant proteins in these samples (Fig EV1A and B). For example, Pum2 was one of the strongest Pum1 interactors in the cortex but turned up in only three out of six of the whole-brain samples (Figs 2A and EV1C, and Dataset EV1) and was expressed at low levels in all brain regions examined (Fig EV1D). These findings suggest that the candidate interactors represent biological information rather than post-lysis effects or degree of expression.

DAVID Gene Ontology analysis revealed that the main functional categories across the three regions were ubiquitin ligases (anaphase-promoting complex [APC/C], E2/E3 and K11-linked ubiquitin), mTOR, and RBPs involved in various aspects of RNA metabolism (RNA silencing, 3'UTR binding, mRNA stability, transport, and splicing; Fig 2B and Dataset EV2). Components of these pathways were consistent across the three brain regions (Fig 2A and B, and Dataset EV1), but the regional analysis expanded the list of Pum1 interactors in several other pathways (Fig 2). For example, Cnot1 turned up in all three brain regions (Fig EV1C), but Cnot2 appeared only in cortex and cerebellum, and Cnot10 only in the cortex (Fig 2A). There were many putative interactors involved in translation initiation, with Eif3b showing up in both the hippocampus and the whole brain (Fig 2A). Splicing factors Rbfox2 and 3 appeared across brain regions, but Rbfox1 was restricted to the cortex (Fig 2A). This is consistent with previous work showing that Rbfox1 mediates cell-type-specific splicing in cortical interneurons (Wamsley *et al*, 2018). Such findings lend further support to the notion that the candidate interactors are not post-lysis artifacts.

We used IP and co-IP to spot-check key candidates from the APC/C (cluster 1: Anapc1, Fzr1) and mTOR (cluster 10: Rptor, Cad) pathways (Figs EV1C and EV2C and D). We tried to purify recombinant proteins, but many of the proteins or their complexes are either quite large (> 100 kD) or strongly tended to aggregate. We were able to confirm direct interactions between Pum1 and recombinant GST-tagged FMRP (Fig EV2A) or GST-tagged PUM2 (Fig EV2B).

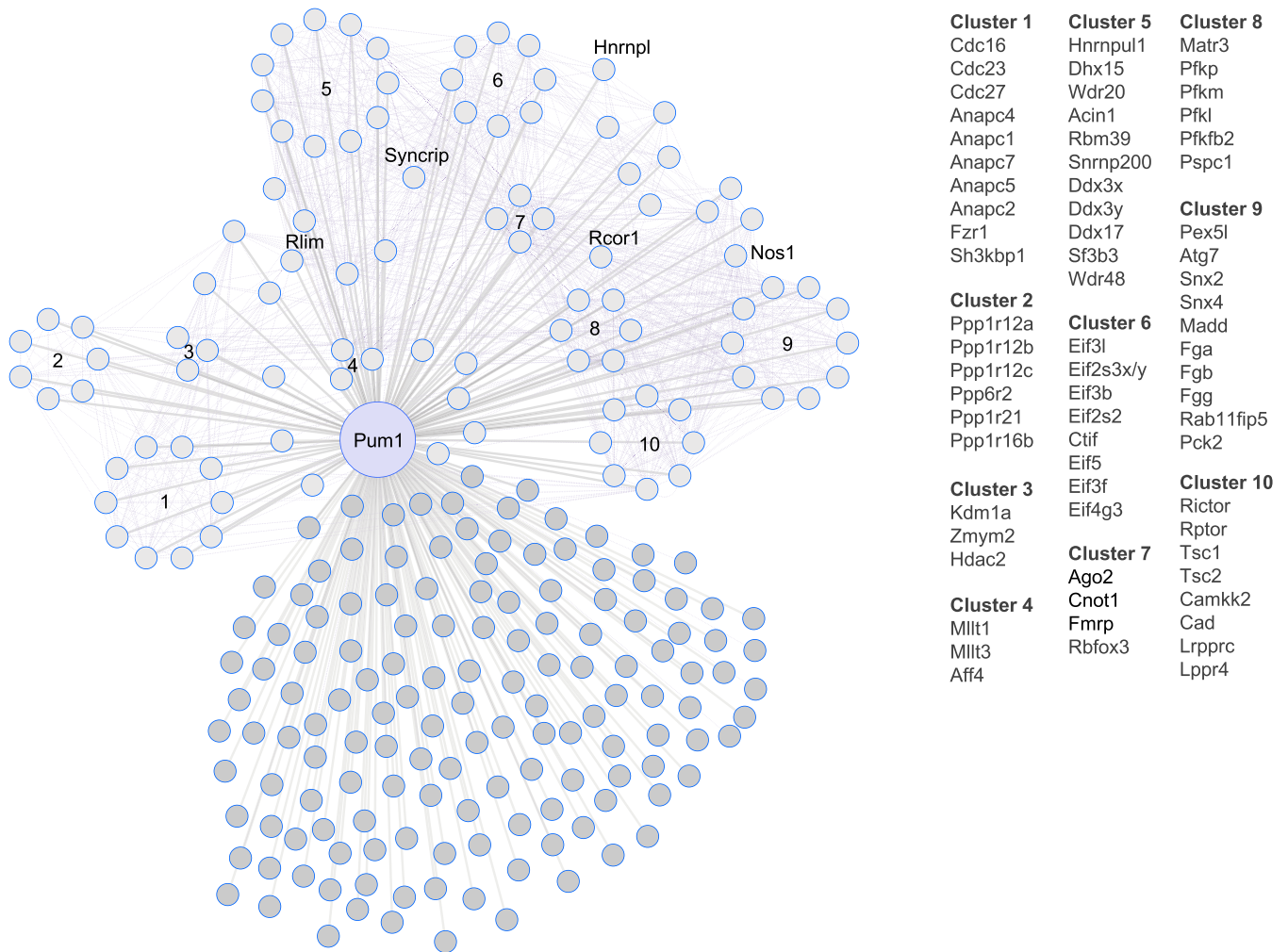


**Figure 1. A brain-specific Pum1 interactome.**

Network of putative Pum1 interactors in 10-week-old mouse brain (circles connected to Pum1 by gray lines). Interactions between interactors (purple lines) were inferred by g:GOST from Corum and the Human Protein Atlas (see [Materials and Methods](#)). The proteins in each of the 10 clusters are listed to the right. We combined and homogenized whole brains from two 10-week-old wild-type mice per sample (one female and one male), aliquoting half of each sample for IP against either Pum1 or IgG, then performed six biological replicates (six samples, 12 mice total) for each LC–MS/MS experiment against IP-Pum1 and IP-IgG. All putative Pum1 interactors are listed in Dataset [EV1](#).

For further *in vivo* study, we decided to prioritize the RBPs in cluster 7 (Fig 1): Fmrp and Ago2 (involved in RNA silencing), Cnot1 (mRNA deadenylase protein), Rbfox3 (alternative splicing factor). We reasoned as follows. First, RBP-RBP interactions are biologically important, and RNA-related categories were prominent in the gene ontology analyses for both the whole brain and all three brain regions. Second, this cluster was the most highly interconnected with other clusters and likely to influence their activities. Third, these RBPs have been well studied, albeit mostly *in vitro*; with the exception of Fmrp (Zhang *et al.*, 2017), they have not been previously associated with Pum1 in the murine brain, so they might shed more light on Pum1 biology. We also decided to study Pum2, which did not pass the stringent threshold of our mass spec studies but is thought to

interact with Fmrp (Zhang *et al.*, 2017), and Mov10, which is known to bind both Fmrp and Ago2 *in vitro* (Kenny *et al.*, 2014, 2020).

#### **Pum1 associates with Fmrp, Ago2, Cnot1, and Pum2 in the absence of mRNA**

We first confirmed that Pum1 associates with Pum2, Fmrp, Ago2, Rbfox3, and Cnot1 by co-IP followed by western blot in 10-week-old mouse brain (Fig 3A, left panel). We found that Mov10 associated with Pum1, likely in concert with Fmrp (Fig 3A). We co-IP'd Pum1 and blotted for all six RBPs in *Pum1*<sup>-/-</sup> mouse brains; none were detected (Fig EV3A). We then tested other proteins associated with the RNA silencing machinery that did not appear in our LC–MS/MS

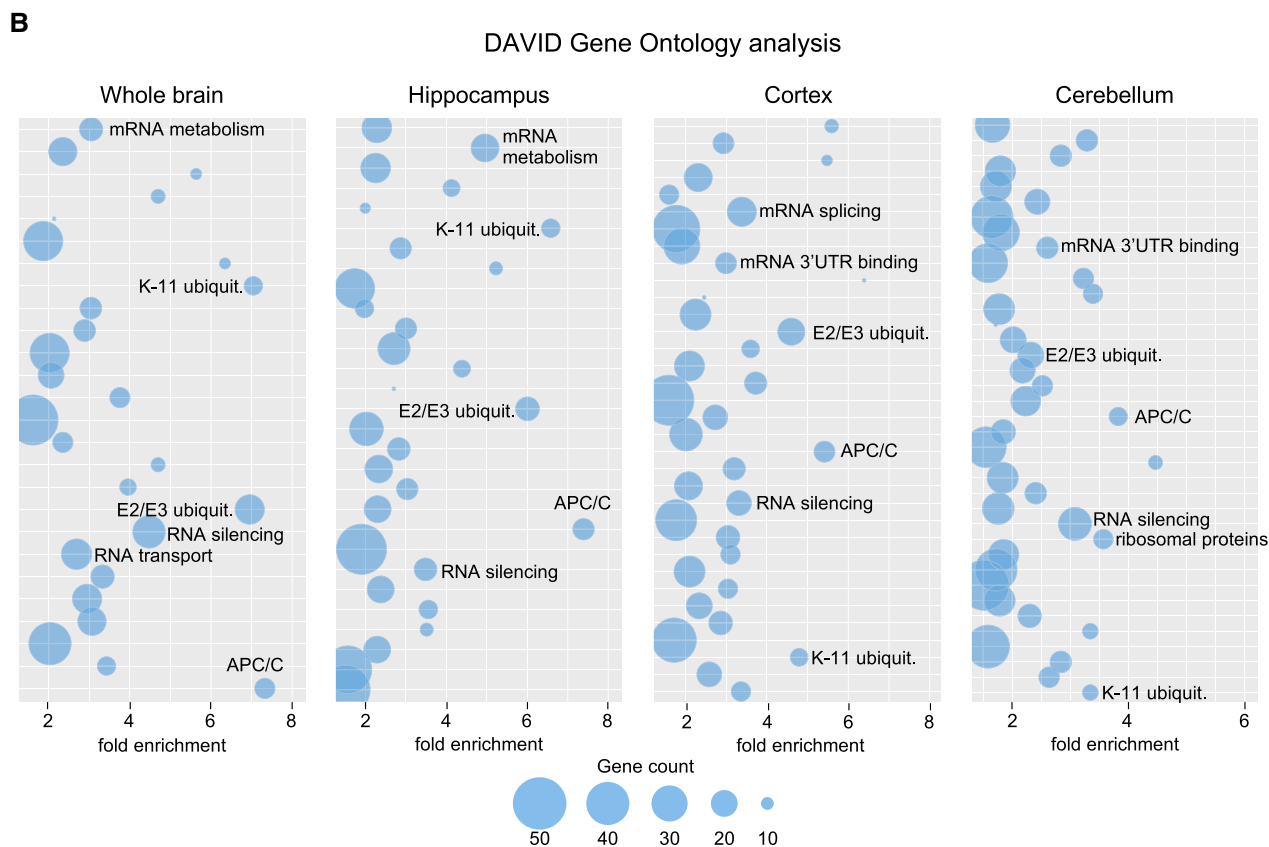
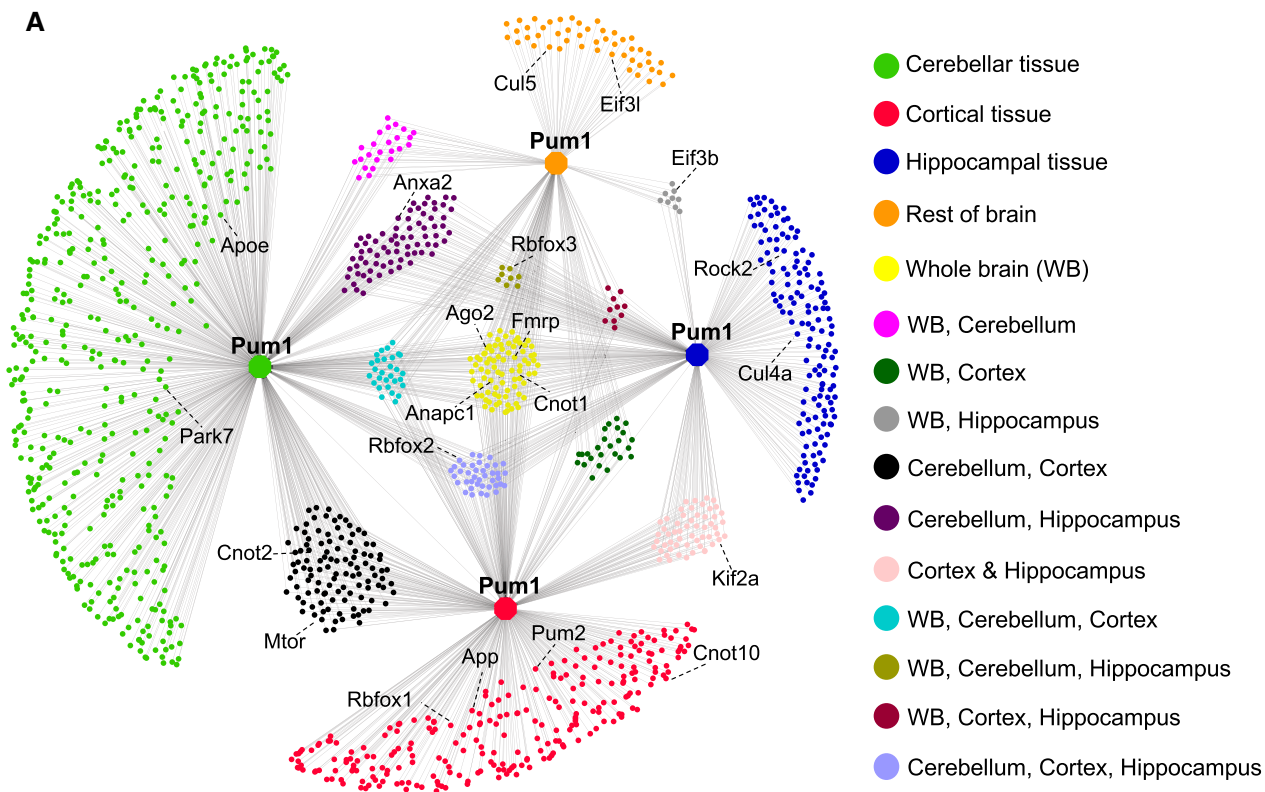
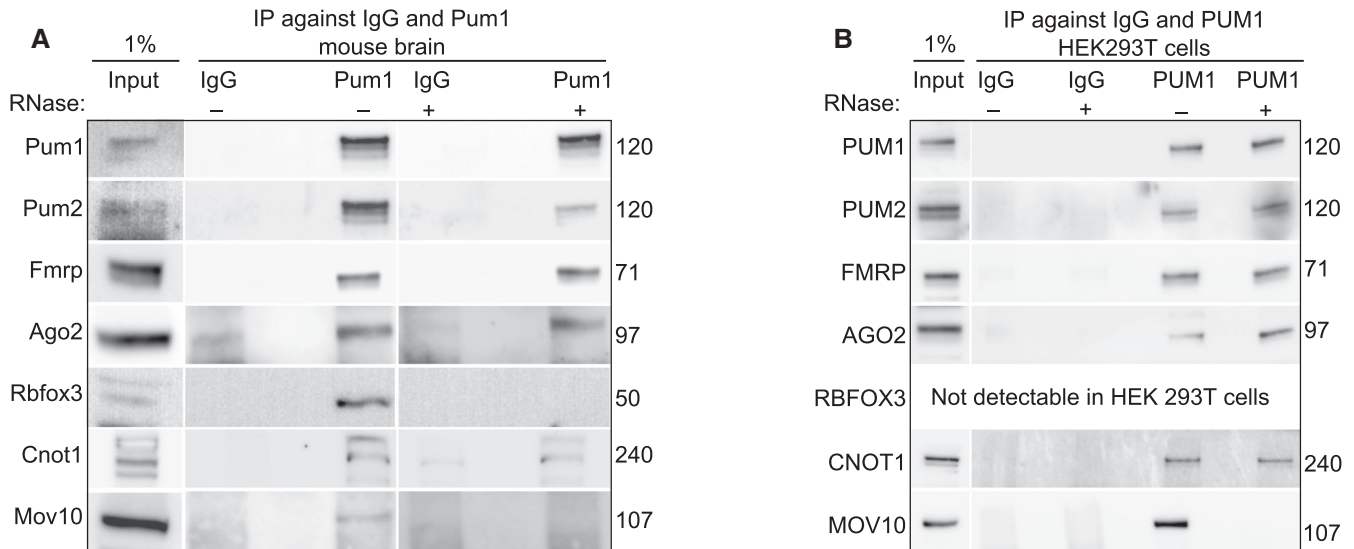


Figure 2.



**Figure 2. A brain-region specific Pum1 interactome.**

- A Pum1 interactome from 10-week-old mouse cerebella ( $n = 8$  mice, four male and four female), hippocampi ( $n = 10$ , 5/5), cortices ( $n = 8$ , 4/4) and the rest of the brain (i.e., excluding those three regions) for a total of 1,500 proteins (Dataset EV1). Node colors represent different brain regions or the overlap between two or more brain regions as noted. All experiments were performed at least in triplicate. IP against IgG was used as a negative control.
- B Bubble plots show the top categories from gene ontology analyses of Pum1 interactors from whole brain, hippocampus, cortex, and cerebellum. Only the categories with fold enrichment  $> 1.5$  and FDR  $< 0.05$  are shown; not all are labeled because of space limitations. The full list of gene ontology categories is available in Dataset EV2.

**Figure 3. Validation of Pum1 associations with RNA-binding proteins in mouse brain.**

- A Representative western blot of proteins pulled down by IP against Pum1 compared with IgG from wild-type mice brain without (left) and with (right) RNase treatment. In this panel, after IP-Pum1, we immunoblotted for Pum1 (positive control), Pum2, Fmrp, Ago2, Rbfox3, Cnot1, and Mov10 (see Materials and Methods).
- B Representative western blots from WT and *Pum1*<sup>-/-</sup> mouse brains, with and without RNase. Molecular weights at the right are in kilodaltons (kDa). All mice were sacrificed at 10 weeks of age. IP against IgG was used as a negative control, and Input (1% from the initial protein lysate; please see Materials and Methods) as a loading control.

data, such as Ago1 and Ago3, and we found no interactions (Fig EV3B).

To exclude the possibility that the co-IP experiments were recovering proteins that co-bound target RNAs but are not part of the same complex as the protein of interest, we treated mouse brain samples with RNase and verified that no detectable RNA remained (see Materials and Methods). Pum1 still associated with Pum2, Fmrp, Ago2, and Cnot1 in the absence of mRNA, but not with Rbfox3 or Mov10 (Fig 3A, right panel). The interactions were confirmed by co-IP against Pum2, Fmrp, Ago2, and Cnot1, followed by western blot for Pum1 in wild-type and *Pum1*<sup>-/-</sup> mice with and without RNase treatment (Fig EV3C). Finally, we repeated the RNase experiments in a human cell line, HEK293T, to confirm our results (Fig 3B). These data suggest that Pum1 interacts with Pum2, Fmrp, Ago2, and Cnot1 prior to binding RNA, in both neurons and other cell types.

**Pum1 loss affects interactor expression by sex and alters miRNA targets in mouse cerebella**

If Pum1 is an important interactor for these six RBPs, loss of Pum1 should affect their abundance or function. *Pum1* heterozygous

and null mice showed changes in the quantities of Pum2, Ago2, and Mov10 proteins across the brain (Fig EV4A), but only *Pum2* showed changes in mRNA levels (Fig EV4B). When we noticed that Ago2 and Mov10 levels fell only in male mice (Fig EV4A), we measured mRNA and protein levels in male and female mice separately. In male null mice, *Fmrp* protein expression was upregulated in all three brain regions, but in female null cerebella *Fmrp* was almost 70% lower (Fig 4A), consistent with previous reports (Singh *et al.*, 2007; Singh & Prasad, 2008). Ago2, Rbfox3, and Cnot1 also showed divergent responses to Pum1 loss according to sex and brain region, but Pum2 protein levels rose in all three brain regions (Fig 4A–C). Despite the fact that *Fmr1* and *Cnot1*, like *Pum2*, have a Pumilio Response Element (PRE) (Zamore *et al.*, 1997) in their 3'UTR, only *Pum2* showed any changes in mRNA levels (Appendix Fig S3).

We next asked whether these changes in abundance had functional consequences. We focused on the cerebellum, where Pum1 loss has particularly important effects (Gennarino *et al.*, 2015, 2018). Because Pum1 is known to interact closely with the miRNA machinery (Kedde *et al.*, 2010), we examined the effects of the changes in Ago2 protein levels on cerebellar miRNAs in male and female mice. We detected 701 miRNA by miRNA-seq that are expressed in both male and female knockout mice (Appendix Fig S4A and B). Many of

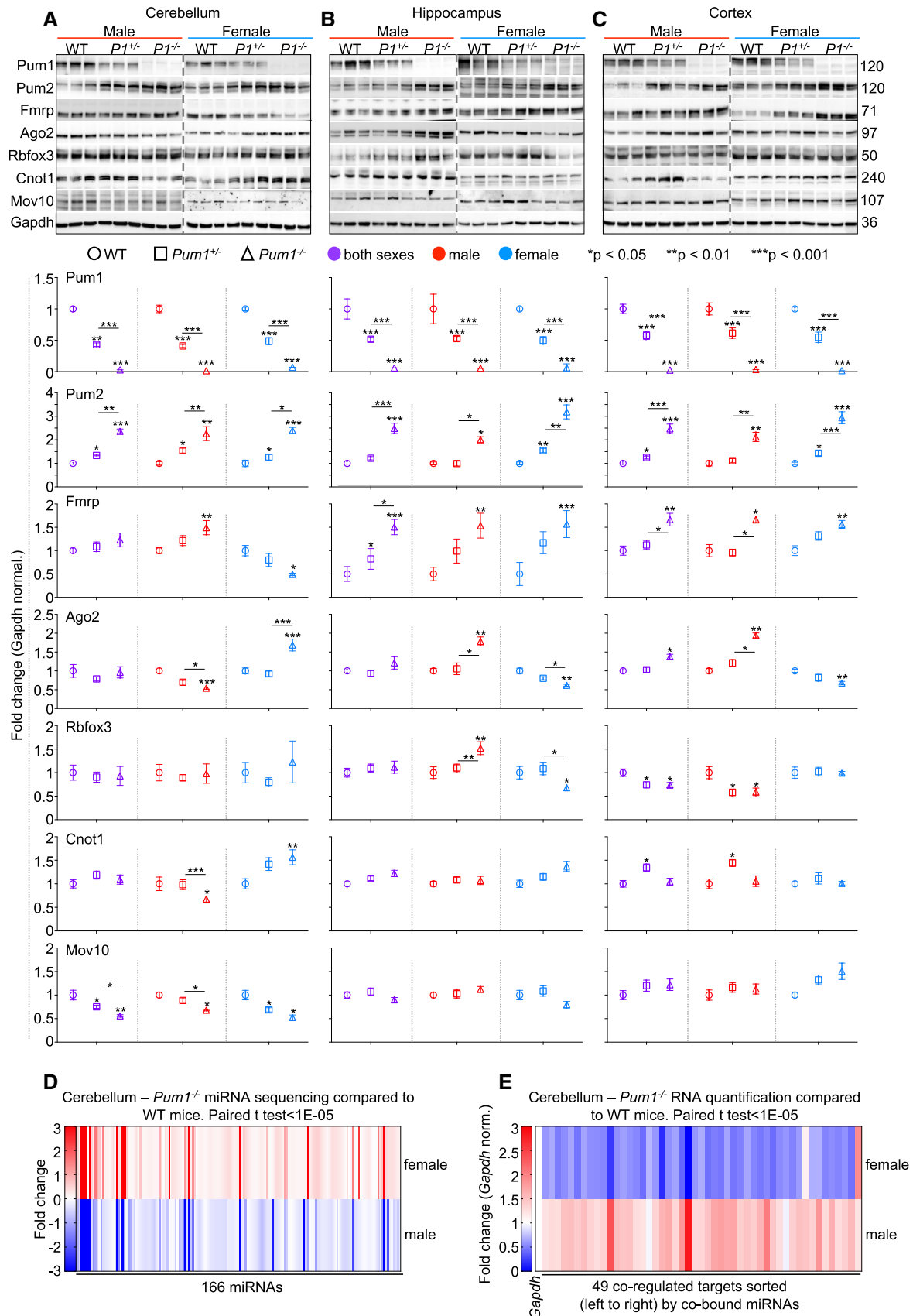


Figure 4.

**Figure 4. Pum1 loss affects Pum1 interactors and the microRNA machinery by brain region and sex.**

- A–C Representative western blots of Pum1, Pum2, Fmrp, Ago2, Rbfox3, Cnot1, and Mov10 in (A) cerebellum, (B) hippocampus, and (C) cortex in both male and female WT, *Pum1*<sup>+/-</sup>, and *Pum1*<sup>-/-</sup> mice. All the experiments were conducted with equal numbers of 10-week-old male and female mice per genotype, for a total of at least 6 mice per genotype (data represent mean ± SEM). To the right are molecular weights in kilodaltons (kDa). Graphs below show quantification for each protein by brain region, sex, and genotype. All data were normalized to Gapdh protein levels. *P* values were calculated by two-tailed Student's *t* test. \**P* < 0.05, \*\**P* < 0.01, \*\*\**P* < 0.001. P1 indicates Pum1. See Appendix Fig S3 for mRNA quantification for each interactor, brain region, and sex.
- D Heatmap showing 166 microRNAs from cerebella of *Pum1*<sup>-/-</sup> male and female mice that were dysregulated (fold change -3 to +3) relative to wild-type cerebellum. The full list of miRNA names and fold changes are available in Dataset EV3. See Appendix Fig S4 for male and female miRNA scatter plots.
- E Heatmap showing mRNA quantification by qPCR for 49 targets co-bound by a minimum of eight dysregulated miRNAs (> 25% change) from panel (D). Statistical significance and magnitude of dysregulation are illustrated for both male and female in Appendix Fig S4. The entire list of targets predicted to be co-bound by at least two miRNAs is presented in Dataset EV4.

these showed differential expression by sex; of these, 166 miRNA diverged significantly (*P* < 0.05) between *Pum1*<sup>-/-</sup> and WT male and female mice in parallel with Ago2 expression (Dataset EV3, Fig 4D). To determine the effects on downstream targets that are co-bound by those miRNAs, we focused on the 49 miRNAs that showed > 25% change in expression in either direction.

Using TargetScan and CoMeTa (Gennarino *et al*, 2012; Agarwal *et al*, 2015) we identified 6,832 putative targets that are co-bound by at least two of these 49 miRNA. To reduce this list to manageable size, we prioritized targets that are co-bound by at least eight of these miRNAs; this yielded, coincidentally, 49 putative targets. In 10-week-old *Pum1*<sup>-/-</sup> male and female cerebella, 44 of these 49 targets showed gene expression changes that correlated with the sex differences in Ago2 levels (Fig 4E, Appendix Fig S5 and Dataset EV4). The disrupted interaction between Pum1 and Ago2 clearly has physiological consequences.

To identify the biological pathways in which these miRNAs play a role, we performed David Gene Ontology (GO) analysis. We decided to select targets bound by at least four of the 49 miRNAs (see Materials and Methods; Appendix Fig S6A–C). The resulting 2,127 targets were enriched for multiple categories having to do with synaptic function under “cellular components.” The most enriched categories under “biological processes” were organ growth and post-embryonic development. Under KEGG pathways, there was a particular enrichment in Wnt signaling, dopaminergic and cholinergic pathways, cancers, and protein ubiquitination.

We then analyzed the same targets by SynGO (Koopmans *et al*, 2019), which uses single-cell data to identify genes that are expressed in specific neurons. SynGO pinpointed 117 presynaptic and 124 postsynaptic targets (Appendix Fig S6D). Among the 166 miRNAs that were inversely expressed between sexes were the entire miR-200 family (miR-200a, miR-220b, miR-200c, miR-141, and miR-429), which regulate targets involved in neurogenesis, glioma, and neurodegenerative diseases (Trumbach & Prakash, 2015; Fu *et al*, 2019). These results are consistent with the cerebellar deficits seen in both PRCA and PADDAS and suggest an intimate relation between Pum1 and Ago2 in the mouse cerebellum.

Although we do not yet have enough patients to determine whether there are sex differences in the human phenotypes resulting from the PADDAS and PRCA mutations, a recent study of PUM1 dosage effects (Lin *et al*, 2019) showed that female heterozygous and knockout mice were smaller than their respective male counterparts. It will be interesting to determine whether there are other sex-dependent differences in the phenotypes.

### The top targets of Pum1, Pum2, Fmrp, Ago2, and Rbfox3 strongly overlap

If the complex Pum1 forms with these RBPs are physiologically relevant, as seen for Ago2 in cerebellum, then they should co-regulate at least some of the same mRNA targets. Indeed, one corollary of the “regulon theory,” which posits that mRNA targets in the same pathway are co-regulated (Keene & Lager, 2005; Keene, 2007a,b; Blackinton & Keene, 2014), is that there should be a discernible set of RBPs that do the co-regulating.

To test this hypothesis, we analyzed all the available high-throughput sequencing UV-cross-linking and immunoprecipitation (HITS-CLIP) data available for the murine brain. These data exist for Fmrp (Maurin *et al*, 2018), Ago2 (Chi *et al*, 2009), Rbfox3 (Weyn-Vanhenhenryck *et al*, 2014), Pum1, and Pum2 (Zhang *et al*, 2017). We then performed gene set enrichment analysis (GSEA) (Subramanian *et al*, 2005) using Fmrp as the basis for comparison because it has the largest dataset. As negative controls, we used HITS-CLIP data from mouse brain for the other four available RBPs that did not show up as Pum1 interactors in our LC-MS/MS: Mbnl2 (Charizanis *et al*, 2012), Nova (Zhang *et al*, 2010), Apc (Preitner *et al*, 2014), and Ptpb2 (Licatalosi *et al*, 2012).

Although the datasets are not perfectly matched (the mice were different ages in some cases; see Materials and Methods), this analysis nonetheless revealed that Pum1 targets were concentrated in the top 5<sup>th</sup> percentile of all Fmrp targets, with an enrichment score (ES) of 0.93 (the maximum is 1) and FDR of 0 (Fig 5A, blue line represents ES). Pum2, Ago2, and Rbfox3 showed nearly identical patterns. There was no significant overlap between the targets of Fmrp and those of any negative control (Nova had the highest ES, but this was only 0.36 with a rank max of 45<sup>th</sup> percentile and FDR = 1; Fig 5B). Neither Pum1 nor its partner RBP targets were enriched among any of the ranked target lists of the negative controls (Appendix Fig S7A).

To ascertain where the highest-ranking Fmrp targets fell among the genes with the highest probability of being Pum1 targets, we divided the Fmrp-ranked target list into 10 equal bins according to percentile. We then repeated GSEA of Pum1 HITS-CLIP data for each bin and found that 648 of the 1,194 (54%) identified Pum1 targets are in the top 10<sup>th</sup> percentile of Fmrp targets, with an ES of 0.8 (Fig 5C). This was also true for Pum2, Ago2, and Rbfox3 (Fig 5C).

We then performed the same analysis using the Pum1 target list as the basis for comparison. We ran GSEA on each of the four Pum1 partners against the list of Pum1 target genes, and each partner's targets were within the top 20% of the Pum1 list (Fig 5D): Fmrp's targets reside in the top 10<sup>th</sup> percentile (with an ES of 0.81), Pum2's

targets within the 16<sup>th</sup> percentile (ES = 0.9), Ago2's targets within the 18<sup>th</sup> percentile (ES = 0.76), and Rbfox3's targets within the 19<sup>th</sup> percentile (ES = 0.67). The four RBPs used here as negative controls have a minimum rank at the 37<sup>th</sup> percentile, and the best ES was 0.26 for Apc; none of the five reached statistical significance (Fig 5D). These analyses demonstrate that there is substantial overlap among the highest-ranked targets of Pum1, Pum2, Fmrp, Ago2, and Rbfox3.

We also studied the targets shared by Pum1, Pum2, Ago2, and Rbfox3 to determine how they distribute within Fmrp. We found an

ES of 0.93 falling within the top 5<sup>th</sup> percentile (Fig 5E); 141 out of 175 common targets were within the top 10<sup>th</sup> percentile (bin1) of Fmrp targets, with 99 within the top 5<sup>th</sup> (Fig 5F). This contrasts with the negative controls, for which the best ES was 0.41 within the top 40<sup>th</sup>–60<sup>th</sup> percentile (Fig 5G). DAVID gene ontology analysis of those 175 common targets between Ago2, Pum1, Pum2, Fmrp, and Rbfox3 revealed pathways enriched in neurons and axonal projections (Appendix Fig S7B and C). Previous studies have shown that Pum1 and Pum2 cooperate with the miRNA machinery to suppress certain targets (Kedde et al, 2010; Gennarino et al, 2015). Among Fmrp

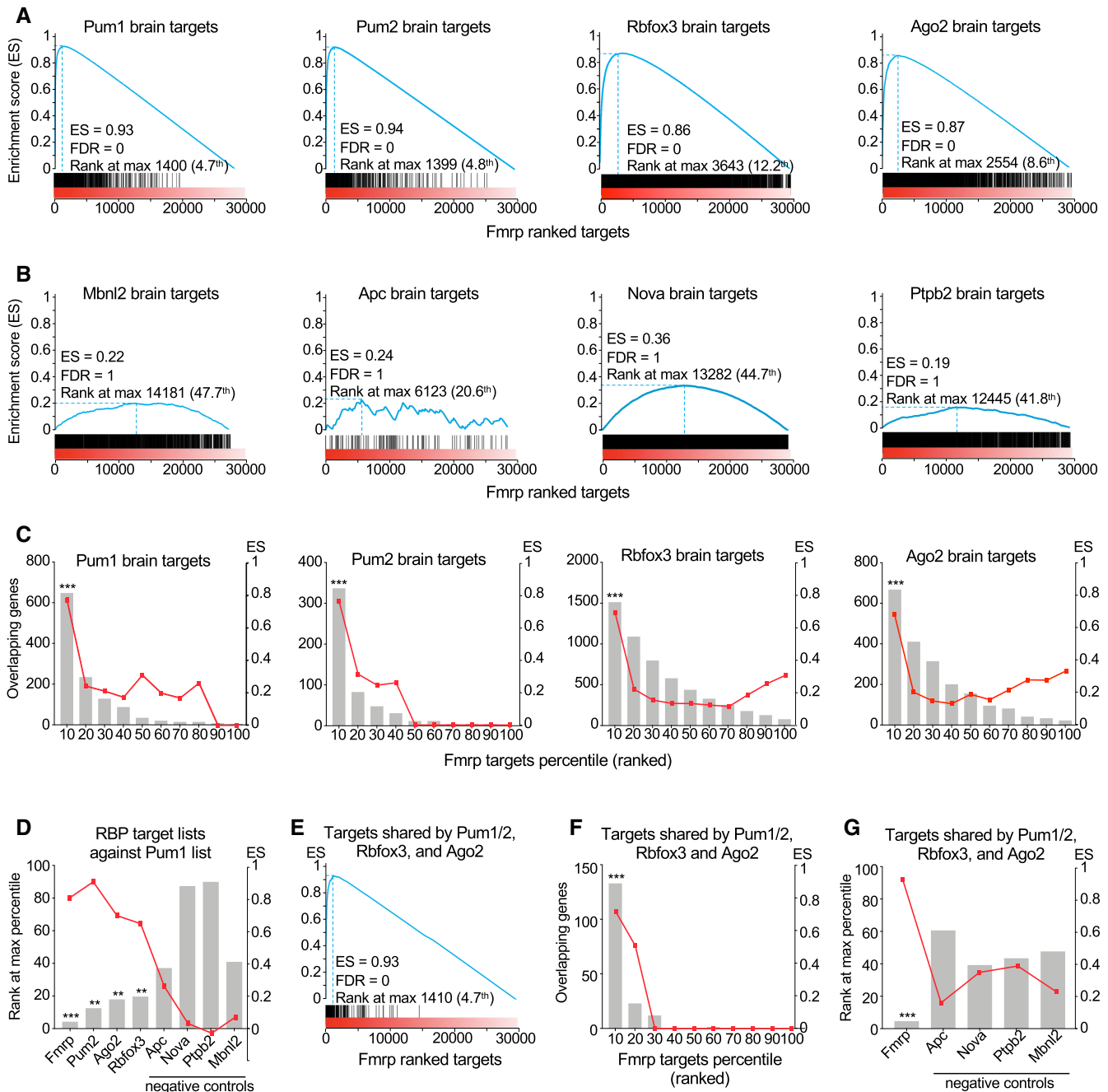


Figure 5.



**Figure 5. Pum1 and its RNA-binding protein interactors share many neuronal mRNA targets.**

- A Enrichment plots generated by Gene Set Enrichment Analysis (GSEA) of Pum1, Pum2, Rbfox3, and Ago2 HITS-CLIP targets plotted against Fmrp ranked HITS-CLIP data. Pum1, Pum2, Rbfox3, and Ago2 targets are enriched at the top 10<sup>th</sup> percentile of the Fmrp targets with FDR = 0.
- B GSEA analysis scores of HITS-CLIP data from each negative control (Apc, Nova, Ptpb2, and Mbnl2) plotted against Fmrp ranked HITS-CLIP data. The negative controls have a maximum enrichment score of 0.36 for Apc ranking at the top 44.7% with FDR = 1.
- C GSEA analysis scores of Pum1, Pum2, Rbfox3, and Ago2 HITS-CLIP data plotted against Fmrp HITS-CLIP data divided into 10-percentile ranked bins shows the shared targets are among the top percentiles of targets for each protein.
- D GSEA analysis scores of the HITS-CLIP data for Fmrp, Pum2, Ago2, Rbfox3, and four negative controls (Apc, Nova, Ptpb2, and Mbnl2) against Pum1 ranked HITS-CLIP data. The targets of Fmrp, Ago2, Pum2, and Rbfox3 are enriched at the top 5<sup>th</sup> to 18<sup>th</sup> percentile of Pum1 targets.
- E GSEA analysis of the shared targets between Pum1, Pum2, Ago2, and Rbfox3 against Fmrp showing that they are enriched in the top 5<sup>th</sup> percentile of Fmrp ranked targets.
- F Pum1, Pum2, Ago2, and Rbfox3 shared targets plotted against Fmrp ranked HITS-CLIP targets and divided into 10-percentile bins show that all of their respective targets are enriched at the top 10<sup>th</sup> percentile of the Fmrp ranked targets.
- G GSEA analysis scores of the targets shared by Pum1, Pum2, Ago2, and Rbfox3 and the four negative controls (Apc, Nova, Ptpb2, and Mbnl2) plotted against Fmrp. At best the negative controls are enriched at the top 40% with a maximum ES of 0.41.

Data information: For all the GSEA analyses, the False Discovery Rate (FDR) was provided by GSEA: \*\*FDR < 0.05 and \*\*\*FDR < 0.01. ES, enrichment score (blue line). Note that lowest rank at max percentage indicates stronger targets in the rank (see [Materials and Methods](#)). HITS-CLIP data, and the respective rank, were obtained from the literature and were initially acquired as follows: Pum1 and Pum2 (Zhang et al, 2017), Fmrp (Maurin et al, 2018), Ago2 (Chi et al, 2009), Rbfox3 (Weyn-Vanhenryck et al, 2014), Nova (Zhang et al, 2010), Ptpb2 (Licatalosi et al, 2012), Mbnl2 (Charizanis et al, 2012), and Apc (Preitner et al, 2014) (see [Materials and Methods](#) for more details). The full list of shared targets is reported in Dataset EV5. Source data are available online for this figure.

HITS-CLIP targets, there were almost 300 microRNAs. Pum1 HITS-CLIP had 60 miRNAs, only four of which were not shared with Fmrp; Pum2 HITS-CLIP had no miRNAs that were not shared with either Pum1 or Fmrp (Appendix Fig S7D and Dataset EV6). The Pum1 interactions with these fellow RBPs are therefore physiologically relevant.

#### **PUM1 interactors are destabilized in cell lines from PADDAS but not PRCA patients**

Having identified Pum1 interactors and shared targets, we were finally in a position to determine whether either the mildest (T1035S) or most severe (R1147W) missense mutations in PUM1 destabilize these key RBP interactors. We compared patient-derived cell lines (lymphoblasts for T1035S, fibroblasts for R1147W) with their respective age-, sex-, and cell type-matched healthy controls. IP (Fig 6A and B) and Co-IP (Appendix Fig S8A and B) followed by western blot to show that our PUM1 antibody purified 100% of PUM1 protein from both patient-derived cell lines.

Co-IP confirmed that PUM1 associates with FMRP, AGO2, CNOT1, and MOV10 in patient cell lines (Fig 6A and B). (We could not study RBFOX3 or PUM2, which were expressed at insufficient concentrations in the patient-derived cells.) As noted previously, T1035S impairs PUM1 RNA-binding activity (Appendix Fig S8C); this variant had no effect on any of these interacting proteins (Fig 6B). On the other hand, the R1147W variant retains RNA-binding activity but impaired PUM1 association with AGO2, MOV10, and CNOT1 (Fig 6A).

To compare the effects of the mutants in the same cell type, we turned to HEK293T cells. GST-tagged AGO2 associated 72% less with Myc-tagged PUM1-R1147W than it did with Myc-tagged PUM1-WT (Fig EV5A), in accord with our observations in the PADDAS cell lines (Fig 6A and B). AGO2 associated with T1035S-PUM1 40% less than with WT *in vitro*, but in patient cell lines AGO2 protein levels did not change across multiple experiments (Fig 6C). CNOT1 interactions were diminished by ~35% with R1147W but not with T1035S (Fig EV5B). We observed no decrease in PUM1 association

with FMRP (Fig EV5C), consistent with our findings in patient-derived cells.

We next asked whether mutants might affect the stability of WT PUM1. Levels of GST-tagged WT PUM1 were unaffected by Myc-PUM1-T1035S but fell by 50% in the presence of Myc-PUM1-R1147W (Fig EV5D). The same results were observed after RNase treatment (Fig EV5E). The combination of lower WT protein levels and R1147W dysfunction explains why the R1147W human phenotype is closer to that of the *Pum1* null mice than to the heterozygous mice.

Lastly, we found that some of the proteins that lose their association with the R1147W variant were reduced in their expression (Fig 6C and D). AGO2 and CNOT1 levels were ~50% lower in the R1147W cell line but unchanged in the T1035S cell line (Fig 6C and D). The mRNA levels of *PUM1*, *AGO2*, and *CNOT1* did not change (Fig EV5F), confirming that the reductions in their respective protein levels were due to the loss of interaction with PUM1-R1147W. The exception was MOV10, whose protein levels were unchanged even though its association with R1147W was reduced (Fig 6A). Collectively, these data suggest that the R1147W variant exerts a dominant-negative effect on PUM1-RBP interactors by destabilizing them.

#### **Expressing WT PUM1 restores interactor levels and shared target regulation in patient cells**

We next tested the effects of the T1035S and R1147W mutations on both shared targets and validated PUM1-specific targets (Chen et al, 2012; Gennarino et al, 2015; Zhang et al, 2017) that are not in the HITS-CLIP data for the other RBPs but are expressed in both fibroblasts and lymphoblasts. PUM1-specific mRNA were dysregulated to very similar extents in PRCA and PADDAS patient cells (Appendix Fig S9A).

Of the 175 targets shared between PUM1, PUM2, AGO2, FMRP, and RBFOX3 (Dataset EV5), 54 were expressed in both R1147W fibroblasts and T1035S lymphoblastoid cells. Fifty-one of those were upregulated in the former but not the latter (Fig 7A), by an average

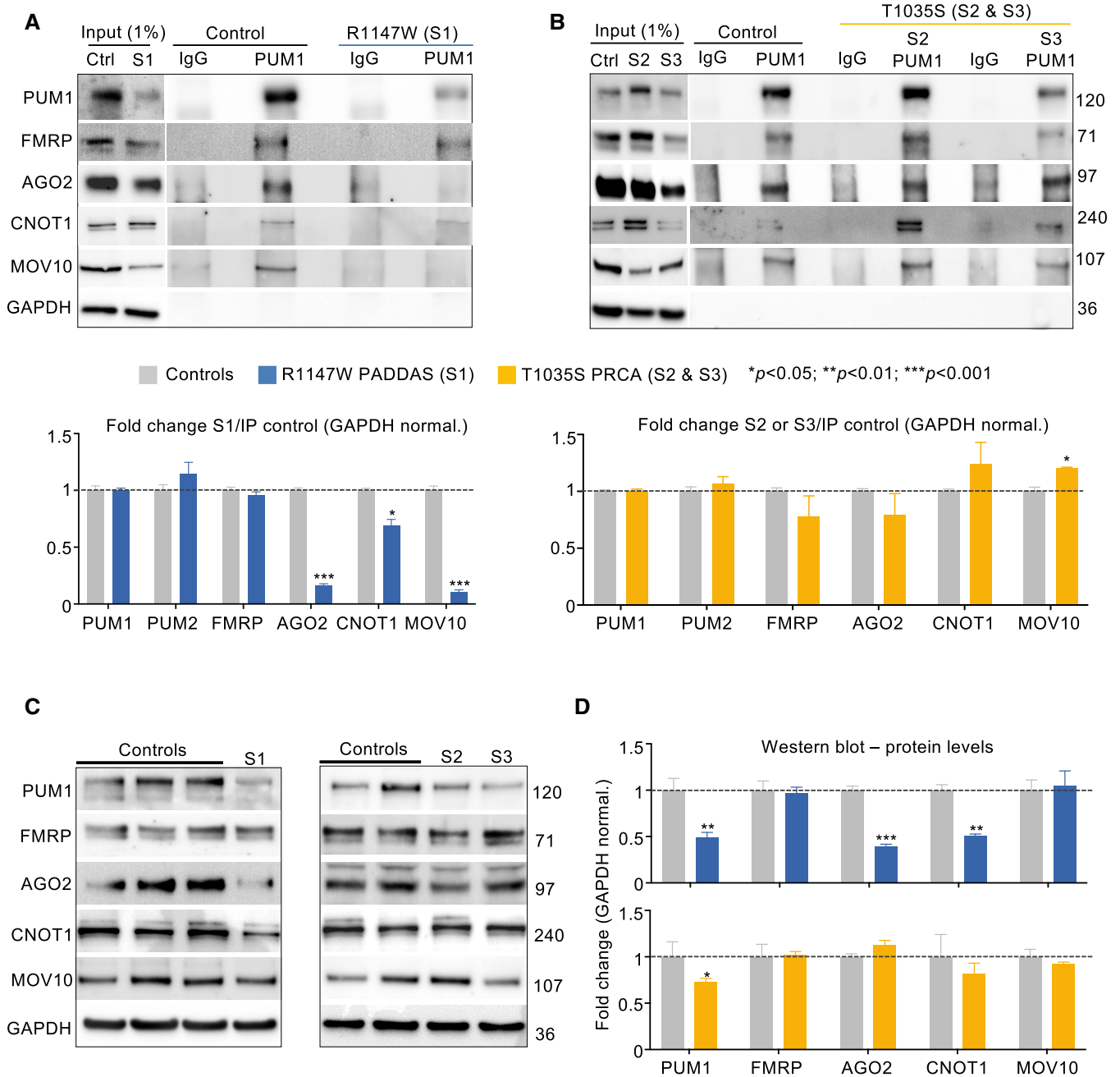


**Figure 6. The R1147W variant, but not T1035S, destabilizes PUM1 interactors.**

A, B IP against PUM1 from Subject 1 (S1, R1147W) (A) and Subject 2 (S2, T1035S) (B) compared with their respective age-, sex-, and cell type- matched healthy controls confirms the interactions between PUM1 (used here as a positive control), and PUM2, FMRP, AGO2, CNOT1, and MOV10. Input (1%) was used as a loading control and IP against IgG was used as a negative control. GAPDH was used here as loading control, see Methods for quantification.

C, D Representative western blots (C) and relative quantification (D) of protein levels for PUM1, PUM2, FMRP, AGO2, CNOT1, and MOV10 in PADDAS patient-derived and PRCA patient-derived cells compared with their respective controls. Data were normalized to GAPDH protein levels.

Data information: From (A) to (C), all the experiments were performed more than three times. Data represent mean  $\pm$  SEM. P values were calculated by two-tailed Student's t test. \* $P < 0.05$ , \*\* $P < 0.01$ , \*\*\* $P < 0.001$ .

Source data are available online for this figure.

of 200% (ranging from a low of 121% for *IDS* to 347% for *TLK1*). There was little or no change in most of these targets in T1035S cells, though levels of *CALM1*, *ATP2A2*, *CREB1*, and *GNAQ* fell by ~40%, and *CALM2*, *TAOK1*, and *UBE2A* by ~20% (Fig 7A).

To determine whether restoring PUM1 levels would normalize expression of these shared targets, we transfected Myc-PUM1-WT in R1147W cells, using transfection with an empty vector as a negative control (Fig 7B, Appendix Fig S9B). WT PUM1 restored AGO2 and

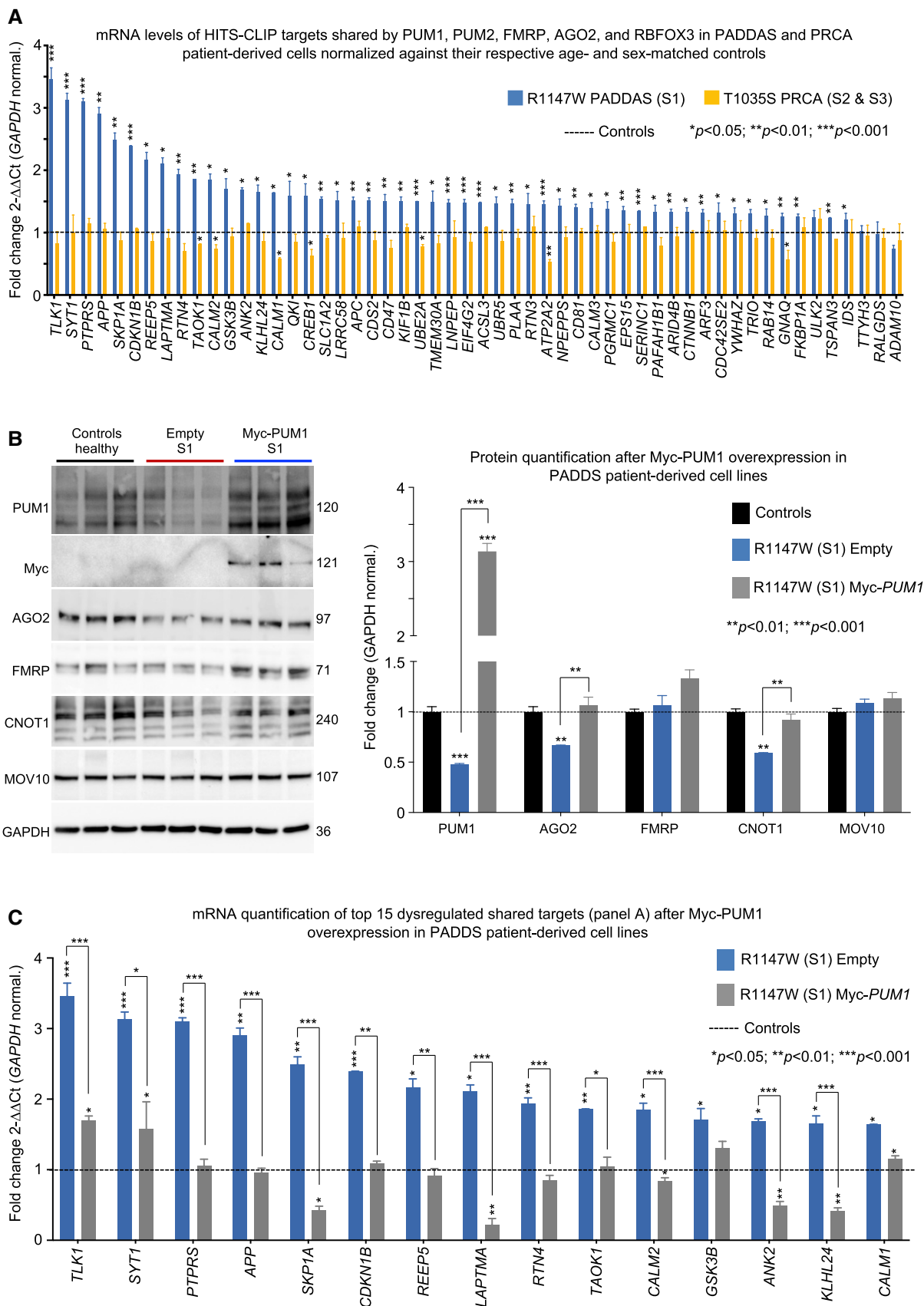


Figure 7.

**Figure 7. Shared targets are upregulated in PADDAS but not in PRCA.**

- A mRNA level quantification of PUM1 neuronal targets in common with FMRP, PUM2, AGO2, and RBFOX3 (Fig 5E and Dataset EV5) in S1 (R1147W, blue bars) and S2 and 3 (T1035S, orange bars) cell lines compared with their respective healthy controls. Only genes expressed in both R1147W and T1035S cell lines are represented here, for a total of 54 genes.
- B Representative western blots (left panel) and relative quantifications (right panel) of PUM1 and its interactors (AGO2, CNOT1, FMRP, and MOV10) in R1147W patient-derived cell lines after Myc-PUM1-WT expression.
- C mRNA quantification of the top 15 shared target genes from panel (A) in R1147W patient-derived cell lines after Myc-PUM1-WT expression.

Data information: All data were normalized to GAPDH mRNA or protein levels and experiments were performed at least three times. Data represent mean  $\pm$  SEM. *P* values were calculated by two-tailed Student's *t* test. \**P* < 0.05, \*\**P* < 0.01, \*\*\**P* < 0.001. The full list of shared targets expressed in fibroblast and lymphoblast cell lines is reported in Dataset EV5.

Source data are available online for this figure.

CNOT1 to wild-type levels, which in turn repressed the top 15 shared targets that were abnormally upregulated in PADDAS cells (Fig 7B and C). These data support the notion that the effects of the R1147W mutation result from disruption of interactions with RBPs that repress the same mRNA targets. These results are also consistent with the hypothesis that the symptoms observed in adult-onset SCA47 (PRCA) are attributable to the dysregulation of PUM1-specific target genes, while infantile-onset SCA47 (PADDAS) involves both protein partner destabilization and dysregulation of the partner proteins' targets.

## Discussion

It seems that for most proteins, the difference in phenotype between greater and lesser abundance reflects a linear progression from mild to severe. For example, a mutation in *MECP2* that reduces its protein levels by only 16% still causes Rett syndrome, just a milder form (Takeguchi *et al*, 2020). Similarly, for proteopathies such as Alzheimer's or Parkinson's disease, genetic duplications of *APP* or *SNCA* cause an earlier onset of what is recognizably the same disease, and triplications cause even more severe forms (Chartier-Harlin *et al*, 2004; Rovelet-Lecrux *et al*, 2006). In the case of PUM1, however, the additional drop in PUM1 levels from PRCA to PADDAS (from 75 to 50% of WT levels) produces phenotypes that appear unrelated to one another. Why should this be so, especially when R1147W is not impaired in binding to mRNA? Although elucidating the pathogenesis of these diseases will require animal models, our data support the molecular hypothesis that the difference between T1035S and R1147W is not due to a linear increase in the derepression of mRNA targets but is rather a function of an additional mechanism coming into play: the destabilization of numerous interactors and the derepression of their downstream targets.

This conclusion relies on five lines of evidence. First, loss of Pum1 in mice affects the abundance of interacting proteins, with some showing differences between brain regions and between male and female mice. The odds of specific proteins consistently appearing in specific brain regions and sexes as false positives, across as many mice as these experiments required, are extremely low. Second, loss of PUM1 also impaired the function of the RBP interactors, whose targets are dysregulated in Pum1-KO mice; moreover, the dysregulation of miRNA showed opposite patterns in male and female cerebella that correlated with the sex-specific patterns of Ago2 expression. Third, the levels of these proteins were reduced 40–70% in PADDAS patient cell lines, despite unaltered mRNA levels, but not

in PRCA patient cells; we also found that 55 shared targets expressed in both lymphoblasts and fibroblasts were derepressed in PADDAS but not PRCA cells. Fourth, our *in vitro* studies showed that AGO2, CNOT1, and WT PUM1 lose their interaction with PUM1-R1147W, but not with T1035S. Fifth, expression of WT PUM1 in PADDAS cell lines restored the abundance of its interactors and repressed downstream targets. These data underscore the importance of examining RBP interactions *in vivo*, in specific contexts (different sex or brain regions), with and without RNase treatment. Our data also suggest that interacting complexes may be disrupted once expression falls below a certain threshold, which for PUM1 appears to be around 50%. It is worth noting that a recent study found that, below a threshold of ~70% of wild-type levels of FMRP, there were steep decreases in IQ for each further 5% decrement in FMRP levels (Kim *et al*, 2019). The amount of loss that can be sustained for a given protein would likely depend on its usual abundance.

Our data also raise the intriguing possibility that the three mechanisms of repression that have been proposed for PUM1—collaborating with the miRNA machinery (Kedde *et al*, 2010; Friend *et al*, 2012; Miles *et al*, 2012), recruiting the CCR4-NOT deadenylase complex to trigger degradation (Van Etten *et al*, 2012; Temme *et al*, 2014; Weidmann *et al*, 2014), and antagonizing poly(A)-binding proteins to repress translation (Goldstrohm *et al*, 2018)—might be coordinated in neurons, insofar as PUM1, PUM2, FMRP, AGO2, MOV10, CNOT1, and RBFOX3 (and related proteins in specific brain regions) either interact or are so close to each other within the ribonucleosome that the loss of Pum1 or RNA can change the composition of the complexes that are identified by co-IP, in ways that are specific to brain region and sex. In this context, it is worth noting that a very recent study found that alternative splicing is altered in hippocampal slices from *Fmrp*-deficient mice; this observation was attributed to changes in H3K36me3 levels (Shah *et al*, 2020), but our data suggest that FMRP has a closer relationship with the RBFOX protein family and alternative splicing machinery than previously imagined. Indeed, recent work has provided tantalizing glimpses of close interactions among various kinds of RNA metabolism. For example, members of the RBFOX family of proteins may, depending on their interactors (and perhaps cell type, sex, age, and species), be involved in microRNA processing in the nucleus and translation in the cytoplasm (Conboy, 2017). The FMRP/MOV10 complex appears to be involved in regulating translation through miRNA, with evidence that this role may change according to cell type (Kenny *et al*, 2020). Another study used quantitative mass spectroscopy to examine how *Fmrp* expression levels change with age in the wild-type rat dentate gyrus and found



differences in the levels of myriad proteins; among the 153 proteins with the most significant changes in levels were Pum1, Pum2 and Pabpc1 (Smidak et al, 2017).

There is still much to be understood about how RNA-binding proteins function and cooperate with each other, particularly *in vivo*. Developing interactomes that are tissue-, age- and even sex-specific should provide a more complex and realistic picture of RNA-binding protein activities in neuronal function and neurological diseases.

## Materials and Methods

### Immunoprecipitation (IP) experiments using mouse brain tissue

Mouse brain tissues were gathered from an equal number of 10-week-old male and female mice. For whole brain experiments, we combined and homogenized two 10-week-old wild-type mouse brains per sample (one female and one male), aliquoting half of each sample for IP against either Pum1 or IgG, then performed six biological replicates (12 mice total) for each LC–MS/MS experiment against IP-Pum1 and IP-IgG. For experiments on the hippocampus, cerebellum, and cortex, we needed much larger numbers of mice: we combined cerebellar and cortical tissues from eight wild-type mice (four male and four female) and performed the experiment in triplicate (total of 24 mice), while for hippocampus we combined tissues from 10 wild-type mice (five female and five male) for three experiments (a total of 30 mice).

Samples were processed with a dounce homogenizer using a lysis buffer consisting of 200 mM NaCl<sub>2</sub>, 100 mM NaPO<sub>4</sub>, 20 mM Hepes pH 7.4, 1% Triton X (which should disrupt all but the strongest protein–protein interactions) and complemented by 1X of Xpert Protease and 1X of Phosphatase Inhibitor Cocktail Solutions (GenDepot, #P3100-100, #P3200-020). Following homogenization, the samples were placed on ice for 15 min and then centrifuged at 14,800 rpm at 4°C for 25 min to remove the debris from the supernatant. The supernatant was then moved to 1.5 ml tubes (Beckman microfuge tube #357448) and spun down in a Beckman ultracentrifuge (Optima Max XP) at 4°C for 25 min at 44,000 rpm. 10% of the protein lysate was stored as input and only 1% was loaded for western blot. The protein extract was later divided into two aliquots, one for IP against the protein of interest (antibodies listed below) and the other for IP against IgG, and was then incubated with 30 µl of Dynabeads™ Protein G (Invitrogen, #10004D) and 5 µg of antibody overnight at 4°C on a rotisserie tube rotator. The next day, the beads were washed four times with the same lysis buffer used for IP and resuspended in 40 µl of elution buffer (consisting of lysis buffer, NuPAGE 10X Reducing Agent [Invitrogen, #NP0009], NuPAGE LDS sample buffer at 1× final concentration [Invitrogen, #NP0007]) and boiled at 95°C for 10 min before the samples were loaded in the NuPAGE 4–12% Bis-Tris Gels (Invitrogen, #NP0335BOX & #NP0336BOX) for further resolution and western blot analysis.

For the IP with RNase treatment, the beads were resuspended in 400 µl of lysis buffer after the three final washes and divided into two separate 1.5 ml tubes of 200 µl each. To establish the dose required to remove all RNA, we tested different amounts of RNase I (Invitrogen, #EN0602) and found that 4 µl was enough to render RNA undetectable both by denaturing gel and cDNA amplification.

This sample and the negative control (i.e., one without RNase treatment) were incubated at 37°C for 15 min on a rotisserie tube rotator. After incubation, all the samples were washed one last time with 500 µl of lysis buffer and then eluted in 20 µl of elution buffer. We used the same protocol for all the IP processed by LC–MS/MS.

The antibodies used for IP were: goat α-PUM1 (Bethyl Laboratories, #A300-201A), rabbit α-PUM2 (Bethyl Laboratories, #A300-202A), rabbit α-FMRP (Abcam Cambridge, #ab17722), rabbit α-AGO2 (Abcam Cambridge, #ab32381), rabbit α-NeuN (Thermo Fisher Scientific, #PA5-37407), rabbit α-CNOT1 (Cell Signaling Technology, #44613), rabbit α-MOV10 (Bethyl Laboratories, #A301-571A), and rabbit α-ANAPC1 (Bethyl Laboratories, #A301-653A).

Please note that *in vivo* IPs from brain lysates present certain challenges that are not encountered *in vitro*. Whereas the total lysate from cells is usually 200–300 µl, the brain lysate must be made in a much larger volume, usually 1.5–2.4 ml, depending on the size of the brain or brain region. This means that in a normal western blot that accommodates 30–40 µl total volume, including reducing buffer and loading blue, we cannot load more than 1–3% from the total brain lysate as input. Therefore, when we pull down a protein of interest (Pum1) and immunoblot for the same protein compared with a standard input (loading the entire IP in one gel), the resulting IP band will be much darker than the input. We then need to expose the Input from the same membrane much longer to visualize it, which is the why we crop the input out from the IPs—this is common practice when working with *in vivo* tissues (Lee et al, 2008, 2020; De Maio et al, 2018; Rousseaux et al, 2018; Sternburg et al, 2018; Di Grazia et al, 2021; Coffin et al, 2022). See also the Source Data showing that the input and the IPs are from the same blot.

### Immunoprecipitation experiments from HEK293T and patient-derived cell lines

HEK293T cells and patient-derived fibroblasts or lymphoblastoid cells were lysed by pipetting up and down with a 1,000 µl tip in a lysis buffer consisting of 200 mM NaCl<sub>2</sub>, 100 mM NaPO<sub>4</sub>, 20 mM Hepes pH 7.4, 1% Triton X and complemented by 1× of Xpert Protease and 1× of Phosphatase Inhibitor Cocktail (GenDepot, #P3100-100, #P3200-020). The rest of the protocol is the same as described above for mouse brain tissue, except that we used 2.5 µg of primary antibody for IP.

### Co-Immunoprecipitation in-gel digestion for LC–MS/MS

Immunoprecipitated samples were separated on NuPAGE 4–12% gradient SDS-PAGE (Invitrogen, #NP0335BOX & #NP0336BOX) and stained with SimplyBlue (Invitrogen, #LC6060). Protein gel slices were excised and *in-gel* digestion performed as previously described (Shevchenko et al, 2006), with minor modifications. Gel slices were washed with 1:1 Acetonitrile and 100 mM ammonium bicarbonate for 30 min then dehydrated with 100% acetonitrile for 10 min until shrunk. The excess acetonitrile was then removed and the slices dried in a speed-vacuum at room temperature for 10 min. Gel slices were reduced with 5 mM DTT for 30 min at 56°C in an air thermostat, cooled down to room temperature, and alkylated with 11 mM IAA for 30 min with no light. Gel slices were then washed with 100 mM of ammonium bicarbonate and 100% acetonitrile for 10 min

each. Excess acetonitrile was removed and dried in a speed-vacuum for 10 min at room temperature and the gel slices were rehydrated in a solution of 25 ng/ $\mu$ l trypsin in 50 mM ammonium bicarbonate for 30 min on ice and digested overnight at 37°C in an air thermostat. Digested peptides were collected and further extracted from gel slices in extraction buffer (1:2 ratio by volume of 5% formic acid: acetonitrile) at high speed, shaking in an air thermostat. The supernatants from both extractions were combined and dried in a speed-vacuum. Peptides were dissolved in 3% acetonitrile/0.1% formic acid.

### Liquid chromatography with tandem mass spectrometry (LC–MS/MS)

The Thermo Scientific Orbitrap Fusion Tribrid mass spectrometer was used for peptide tandem mass spectroscopy (MS/MS). Desalted peptides were injected in an EASY-Spray™ PepMap™ RSLC C18 50 cm X 75 cm ID column (Thermo Scientific) connected to the Orbitrap Fusion™ Tribrid™. Peptide elution and separation were achieved at a non-linear flow rate of 250 nl/min using a gradient of 5–30% of buffer B (0.1% [v/v] formic acid, 100% acetonitrile) for 110 min, maintaining the temperature of the column at 50°C during the entire experiment. Survey scans of peptide precursors are performed from 400 to 1,500  $m/z$  at 120 K full width at half maximum (FWHM) resolution (at 200  $m/z$ ) with a  $2 \times 10^5$  ion count target and a maximum injection time of 50 ms. The instrument was set to run in top speed mode with 3-s cycles for the survey and the MS/MS scans. After a survey scan, MS/MS was performed on the most abundant precursors, i.e., those ions that had a charge state between 2 and 6, and an intensity of at least 5,000, by isolating them in the quadrupole at 1.6 Th. We used collision-induced dissociation (CID) with 35% collision energy and detected the resulting fragments with the rapid scan rate in the ion trap. The automatic gain control (AGC) target for MS/MS was set to  $1 \times 10^4$ , and the maximum injection time was limited to 35 ms. The dynamic exclusion was set to 45 s with a 10 ppm mass tolerance around the precursor and its isotopes. Monoisotopic precursor selection was enabled.

### LC–MS/MS data analysis

Raw mass spectrometric data were analyzed using the MaxQuant environment v.1.6.1.0 (Cox & Mann, 2008) and Andromeda for database searches (Cox et al, 2011) at default settings with a few modifications. The default was used for first search tolerance and main search tolerance (20 and 6 ppm, respectively). MaxQuant was set up to search with the reference mouse proteome database downloaded from Uniprot (<https://www.uniprot.org/proteomes/UP000000589>). MaxQuant searched for trypsin digestion with up to two missed cleavages. Peptide, site, and protein false discovery rates (FDRs) were all set to 1% with a minimum of one peptide needed for identification; label-free quantitation (LFQ) was performed with a minimum ratio count of 1. The following modifications were used for protein quantification: oxidation of methionine (M), acetylation of the protein N-terminus, and deamination for asparagine or glutamine (NQ). Results obtained from MaxQuant were further analyzed using the Perseus statistical package (Tyanova et al, 2016) that is part of the MaxQuant distribution. Protein identifications were

filtered for common contaminants. Proteins were considered for quantification only if they were found in at least two replicate groups. Significant alterations in protein abundance were determined by ANOVA with a threshold for significance of  $P < 0.05$  (permutation-based FDR correction). Pum1 protein interactors were later considered if they were found in at least five out of six LC–MS/MS experiments for whole brain and in at least two out of three experiments for each respective brain region with a fold-change of  $> 1.5$  between LFQ-PUM1-WT and LFQ-IgG-WT (see Dataset EV1).

### Protein–protein interaction map

The protein–protein interaction map for the whole brain (Fig 1) was generated by Cytoscape (<https://cytoscape.org/>; Otasek et al, 2019) and interactions or functional relationships (clusters) were inferred from Corum (Giurgiu et al, 2019) and the Human Protein Atlas (Thul et al, 2017) by g:GOST, which is a package of g:Profiler (<https://biit.cs.ut.ee/gprofiler/gost>; Raudvere et al, 2019). The brain region-specific map (Fig 2A) was generated by Cytoscape (Shannon et al, 2003).

### Quantitative proteomics from mouse brain regions

#### Tissue processing for LC–MS/MS measurements

Frozen brain tissues were weighted and 25–50 mg (dry weight) per sample were cryopulverized and lysed in Urea Buffer (8 M Urea, 75 mM NaCl, 50 mM Tris/HCl pH 8.0, 1 mM EDTA) in a final 1:10 (mg/ $\mu$ l) tissue:buffer ratio. Protein concentration was determined by BCA assay (Pierce). 40  $\mu$ g of total protein per sample was processed further. Disulfide bonds were reduced with 5 mM dithiothreitol and cysteines were subsequently alkylated with 10 mM iodoacetamide. Samples were diluted 1:4 with 50 mM Tris/HCl (pH 8.0) and sequencing grade modified trypsin (Promega) was added in an enzyme-to-substrate ratio of 1:50. After 16 h of digestion, samples were acidified with 1% formic acid (final concentration). Tryptic peptides were desalted on C18 StageTips according to (Rappsilber et al, 2007) and evaporated to dryness in a vacuum concentrator. Dried peptides were then reconstituted in 3% ACN/0.2% Formic acid to a final concentration of 0.5  $\mu$ g/ $\mu$ l.

#### LC–MS/MS analysis on a Q-Exactive HF

About 1  $\mu$ g of total peptides were analyzed on a Waters M-Class UPLC using a 25 cm Thermo Scientific PepMap RSLC C18 2  $\mu$ m 25 cm column coupled to a benchtop Thermo Fisher Scientific Orbitrap Q Exactive HF mass spectrometer. Peptides were separated at a flow rate of 400 nl/min with a 160 min gradient, including sample loading and column equilibration times. Data were acquired in data independent mode using Xcalibur software. MS1 Spectra were measured with a resolution of 120,000, an AGC target of  $5e6$ , and a mass range from 300 to 1,800  $m/z$ . MS2 spectra were measured in 47 segment windows per MS1, each with an isolation window width of 32  $m/z$  (0.5  $m/z$  overlap with the neighboring window), a resolution of 30,000, an AGC target of  $3e6$ , and a stepped collision energy of 22.5, 25, 27.5.

All raw data were analyzed with SpectroNaut software version 15.6.211220 (Biognosys) using a directDIA method based on a UniProt mouse database (release 2014\_07, *Mus musculus*), performed with the “BGS factory settings” including the following

parameters: Oxidation of methionine and protein N-terminal acetylation as variable modifications; carbamidomethylation as fixed modification; Trypsin/P as the digestion enzyme; For identification, we applied a maximum FDR of 1% separately on protein and peptide level. “Cross run normalization” was activated. This gave intensity values for a total of 5,699 protein groups across all samples and replicates. “PG.Quantity” (normalized across samples) values were used for all subsequent analyses.

### Protein purification of recombinant proteins

Recombinant FMRP, PUM2, and PUM1 were purified from *Escherichia coli* BL21-Codon Plus (DE3)-RIL cells. Both FMRP and PUM2 were expressed with an N-terminal GST tag and isolated from the cell lysate using Glutathione Sepharose 4B (GS4B) resin. The proteins were further subjected to size exclusion chromatography using 20 mM HEPES pH 8.0, 200 mM NaCl, and 1 mM DTT as the buffer. MBP-SNAP-PUM1-His<sub>6</sub> was expressed and purified similar to the previously described protocol (Elguindy & Mendell, 2021). After nickel affinity chromatography, MBP-SNAP-PUM1-His<sub>6</sub> was buffer exchanged into 20 mM HEPES pH 8.0, 200 mM NaCl, and 1 mM DTT using PD-10 desalting columns.

### GST pull-down assay

500 mM of purified GST-PUM2 or GST-FMRP was incubated with 1 μM of HIS-PUM1 with 30 μl of Glutathione Sepharose 4B GST-tagged protein purification resin (Cytiva, #17075601) in a final volume of binding buffer (20 mM HEPES pH 8.0, 200 mM NaCl, 0.5% Tween-20) for 1 h at 4°C on the rocker. Resins were washed 3 times in binding buffer and centrifuged at 4,000 g at 4°C; resins were resuspended in 30 μl of elution buffer—which consisted of binding buffer, NuPAGE 10× Reducing Agent (Invitrogen, #NP0009), and NuPAGE LDS sample buffer at 1X final concentration (Invitrogen, #NP0007)—and boiled at 95°C for 10 min before the samples were loaded in the NuPAGE 4–12% Bis-Tris Gels (Invitrogen, #NP0335BOX & #NP0336BOX) for further resolution and western blot analysis. 500 mM of purified GST-PUM2, GST-FMRP, and HIS-PUM1 were used as input controls; GST-PUM2 and GST-FMRP were visualized using rabbit α-GST antibody (1:1,000 [Cell Signaling Technologies, #2625]), whereas for HIS-PUM1 we used rabbit α-HIS Tag antibody (1:3,000 [Cell Signaling Technologies, #2365]).

### Protein quantification for immunoprecipitation and western blot analysis

Patient-derived lymphoblastoid, fibroblast cell lines, and control cell lines were collected at  $6 \times 10^6$  cell confluence and processed for protein extraction. For mouse tissues, we processed either half of the whole brain (the other half was processed for RNA extraction, see below) or the entire hippocampus, cortex, or cerebellum for protein extraction. Mouse tissues or cell pellets were subsequently lysed with modified RIPA buffer consisting of 25 mM Tris-HCl, pH 7.6, 150 mM NaCl, 1.0% Tween 20, 1.0% sodium deoxycholate, 0.1% SDS, completed with 1X Xpert Protease and 1X Phosphatase Inhibitor Cocktail Solutions (GenDepot, #P3100-100 & #P3200-020). Cells were lysed by pipetting them up and down with a p1000 tip and then placed on ice for 20 min followed by centrifugation at 14,800

rpm at 4°C for 25 min. Mouse brain tissues were pipetted up and down by syringe needles—starting from an 18G 1½” (Becton Dickson, #305196), moving to 21G 1½” (Becton Dickson, #305167) and finally to a 26G 1½” (Becton Dickson, #305111) needle—until the lysate passed through the needle smoothly. Proteins were quantified by Pierce BCA Protein Assay Kit (Thermo Scientific, #PI23225) and their absorbance measured by NanoDrop OneC (Thermo Scientific). Proteins were resolved by high-resolution NuPAGE 4–12% Bis-Tris Gel (Invitrogen, #NP0335BOX & #NP0336BOX) according to the manufacturer’s instructions. All the blots were acquired on the G:BOX Chemi XX9 machine (Syngene; Frederick, MD) using GeneSys software 1.6.5.0. Gel exposures were determined by the software.

To calculate the fold-change of a given protein in Subject cell lines relative to controls, we compared the ratio of the change in the protein of interest relative to PUM1 in controls (between IP and input lanes, normalized to GAPDH), divided by the ratio of the change in the same protein relative to PUM1 in the Subject (also between IP and input lanes, and also normalized to GAPDH). Written as a formula, where x represents the protein of interest, this would be:

$$\text{Fold Change (FC)} = \frac{\text{Subject} \left\{ \frac{[\text{IP}^x \div (\text{Input}^x \div \text{GAPDH})]}{[\text{IP}^{\text{PUM1}} \div (\text{Input}^{\text{PUM1}} \div \text{GAPDH})]} \right\}}{\text{Control} \left\{ \frac{[\text{IP}^x \div (\text{Input}^x \div \text{GAPDH})]}{[\text{IP}^{\text{PUM1}} \div (\text{Input}^{\text{PUM1}} \div \text{GAPDH})]} \right\}}$$

Antibodies used for western blot experiments were: goat α-PUM1 (1:2,500 [Bethyl Laboratories, #A300-201A]), rabbit α-PUM1 (1:2,000 [Abcam Cambridge, #ab92545]), rabbit α-PUM2 (1:2,000 [Bethyl Laboratories, #A300-202A]), rabbit α-FMRP (1:1,000 [Abcam Cambridge, #ab17722]), rabbit α-AGO2 (1:1,000 [Abcam Cambridge, #ab32381]), rabbit α-NeuN (Rbfox3) (1:1,000 [Thermo Scientific, #PA5-37407]), rabbit α-CNOT1 (1:1,000 [Cell Signaling Technology, #44613]), rabbit α-MOV10 (1:2,000 [Bethyl Laboratories, #A301-571A]), and mouse α-GAPDH (1:10,000 [Millipore, #CB1001]).

### HEK293T cell culture and maintenance

Human embryonic kidney immortalized 293T (HEK293T) cells were grown in DMEM (GenDepot, #CM002-320) supplemented with 10% of heat-inactivated fetal bovine serum (FBS [GenDepot, #F0901-050]) and 1% penicillin/streptomycin (GenDepot, #CA005-010). All cells were incubated at 37°C in a humidified chamber supplemented with 5% CO<sub>2</sub>. HEK293T cells were later processed according to the needs of specific experiments (described below).

### RNA extraction and quantitative real-time PCR (qPCR)

Human fibroblast, lymphoblastoid, and respective control cell lines were harvested at  $6 \times 10^6$  confluence prior to RNA extraction. For mouse tissues, half of the whole brain (the other half was processed for protein extraction, see above) or the entire hippocampus, cortex, or cerebellum was processed for RNA extraction. The RNA was collected for both human cells, mouse brain and brain region tissues using the miRNeasy kit (QIAGEN, # 217004) according to the manufacturer’s instructions. RNA was quantified using NanoDrop OneC

(Thermo Fisher Scientific). cDNA was synthesized using Quantitect Reverse Transcription kit (QIAGEN, # 205313) starting from 1 µg of RNA. Quantitative RT-polymerase chain reaction (qRT-PCR) experiments were performed using the CFX96 Touch Real-Time PCR Detection System (Bio-Rad Laboratories, Hercules) with PowerUP SYBR Green Master Mix (Applied Biosystems, #A25743). Real-time PCR runs were analyzed using the comparative  $C_T$  method normalized against the housekeeping human gene *GAPDH* or mouse *Gapdh*, depending on the experiment (Vandesompele et al, 2002).

### RNA immunoprecipitation (RIP)

HCT116 wild-type and PUM1-KO were obtained from (Lee et al, 2016). HCT116-PUM1-KO cells were grown in McCoy's 5A Media (Merck, # M4892) supplemented with 10% of heat-inactivated fetal bovine serum (FBS [GenDepot, #F0901-050]) and 1% penicillin/streptomycin (GenDepot, #CA005-010) for 16 h in a 10-cm plate (80% confluency) and transfected with 6 µg of Myc-PUM1-WT, Myc-PUM1-R1147W, and Myc-PUM1-T1035S. After 48 h cells were collected and lysed in Polysome Lysis Buffer (PLB) (10 mM HEPES-KOH pH 7, 100 mM KCl, 5 mM MgCl<sub>2</sub>, 25 mM EDTA, 0.5% NP40, 2 mM Dithiothreitol, 0.2 mg/ml Heparin) supplemented with 50 U/ml of RNase OUT™ recombinant ribonuclease inhibitor (Thermo Fischer Scientific, # 10777019), 50 U/ml of SuperaseIN™ RNase inhibitor (Thermo Fischer Scientific, #AM2694) and 1X of Xpert Protease Inhibitor Cocktail Solutions (GenDepot, #P3100-100) for 20 min in ice; cells were centrifuged at maximum speed at 4°C to remove cellular debris. 5 µg of goat α-PUM1 (Bethyl Laboratories, #A300-201A) or α-Goat-IgG with 50 µl of Dynabeads™ Protein G (Invitrogen, #10004D) was incubated overnight at 4°C on a rotisserie tube rotator; 100 µl of lysate was removed to serve as input. 3 mg of lysate with 10 µl of Dynabeads™ Protein G (Invitrogen, #10004D) was pre-cleared for 30 min at 4°C on a rotisserie tube rotator; the pre-cleared lysate was incubated with antibody-conjugated beads overnight at 4°C on a rotisserie tube rotator. Beads were washed 3 times with NT2 buffer (50 mM of Tris-HCl, 300 mM NaCl, 1 mM EDTA, 1% NP40, 0.1% SDS, 0.5% Na-deoxycholate supplemented with 1× of Xpert Protease Inhibitor Cocktail Solutions). Beads and input were resuspended in 100 µl of NT2 buffer supplemented with 80 U of RNase OUT and 30 µg of proteinase K and incubated for 30 min at 50°C to eliminate the proteins. RNA was extracted from the immunoprecipitated samples and their input; 200 µl of RLT buffer was added using RNeasy Mini Kit (Qiagen, #74104) according to the manufacturer's instruction. cDNA was synthesized using SuperScript™ II Reverse Transcriptase (Thermo Fisher Scientific, #18064014) according to the manufacturer's instructions. Quantitative RT-polymerase chain reaction (qRT-PCR) experiments were performed using the CFX96 Touch Real-Time PCR Detection System (Bio-Rad Laboratories, Hercules) with PowerUP SYBR Green Master Mix (Applied Biosystems, #A25743). The oligos used for qPCR are listed in Dataset EV7.

### microRNA library construction and sequencing

Library preparation and microRNA sequencing were performed by LC Sciences (Houston, TX) according to the following criteria. Total RNA was extracted from cerebellum of WT and *Pum1*<sup>-/-</sup> male and female at 10 weeks of age using the miRNeasy kit (QIAGEN, #

217004) according to the manufacturer's instructions. The total RNA quality and quantity were assessed with Bioanalyzer 2100 (Agilent Technologies, Santa Clara) with RIN number > 7.0. Approximately 1 µg of total RNA was used to prepare the small RNA library according to the protocol of TruSeq Small RNA Sample Prep Kits (Illumina, San Diego). Then the single-end sequencing 50 bp was performed on an Illumina HiSeq 2500 at LC Sciences (Hangzhou, China) following the vendor's recommended protocol.

Labelling scheme:

Sample	Gender	Genotype
LCS7846_GV_KO1_F	Female	KO
LCS7846_GV_KO1_M	Male	KO
LCS7846_GV_KO2_M	Male	KO
LCS7846_GV_KO3_F	Female	KO
LCS7846_GV_KO3_M	Male	KO
LCS7846_GV_KO4_F	Female	KO
LCS7846_GV_WT1_M	Male	WT
LCS7846_GV_WT2_F	Female	WT
LCS7846_GV_WT2_M	Male	WT
LCS7846_GV_WT3_F	Female	WT
LCS7846_GV_WT3_M	Male	WT

### microRNA sequencing bioinformatic analysis

Raw reads were subjected to an in-house program, ACGT101-miR (LC Sciences, Houston), to remove adapter dimers, junk, common RNA families (rRNA, tRNA, snRNA, snoRNA), and repeats. Subsequently, unique sequences of 18–26 nucleotides in length were mapped to specific species precursors in miRBase 22.0 (<http://www.mirbase.org/>) by BLAST search to identify known miRNAs and novel 3p- and 5p-derived miRNAs. Length variation at both 3' and 5' ends and one mismatch inside of the sequence were allowed in the alignment. The unique sequences mapping to specific species of mature miRNAs in hairpin arms was identified as known miRNAs. The unique sequences mapping to the other arm of known specific species precursor hairpins opposite the annotated mature miRNA-containing arm was considered to be novel 5p- or 3p-derived miRNA candidates. The remaining sequences were mapped to other selected species precursors (with the exclusion of specific species) in miRBase 22.0 by BLAST search, and the mapped pre-miRNAs were further BLASTed against the specific species genomes to determine their genomic locations. The last two were also defined as known miRNAs. The unmapped sequences were BLASTed against the specific genomes, and the hairpin RNA structures containing sequences were predicted from the flank 80 nt sequences using RNAfold software (<http://rna.tbi.univie.ac.at/cgi-bin/RNAWebSuite/RNAfold.cgi>). The criteria for secondary structure prediction were: (1) number of nucleotides in one bulge in stem ( $\leq 12$ ), (2) number of base pairs in the stem region of the predicted hairpin ( $\geq 16$ ), (3) cutoff of free energy (kCal/mol  $\leq -15$ ), (4) length of hairpin (up and down stems + terminal loop  $\geq 50$ ), (5) length of hairpin loop ( $\leq 20$ ), (6) number of nucleotides in one bulge in mature region ( $\leq 8$ ), (7) number of biased errors in one bulge in



mature region ( $\leq 4$ ), (8) number of biased bulges in mature region ( $\leq 2$ ), (9) number of errors in mature region ( $\leq 7$ ), (10) number of base pairs in the mature region of the predicted hairpin ( $\geq 12$ ), (11) percent of mature region in stem ( $\geq 80$ ).

### Gene set enrichment analysis (GSEA)

GSEA was performed as previously described (Subramanian et al, 2005). The cumulative distribution function was conducted by performing 1,000 random gene-set membership assignments. A nominal  $P$ -value  $< 0.01$  and an FDR  $< 0.25$  were used to assess the significance of the enrichment score (ES). HITS-CLIP data, and the respective rank, were obtained from the literature and were initially acquired as follows: *Pum1* and *Pum2* from neonatal murine brains (Zhang et al, 2017), *Fmrp* from the cerebellum, cortex, and hippocampus together (Maurin et al, 2018), *Ago2* from neocortex at embryonic day 13 (Chi et al, 2009), *Rbfox3* from mouse brain (age not specified) (Weyn-Vanhenhenryck et al, 2014), *Nova* from mouse brain (age not specified) (Zhang et al, 2010), *Ptpb2* from neocortex at embryonic day 18.5 (Licatalosi et al, 2012), *Mbnl2* from hippocampus at 8–12 weeks of age (Charizanis et al, 2012), and *Apc* from mouse brain at embryonic day 14 (Pretner et al, 2014).

### Gene ontology analyses

Gene ontology analyses were performed with David Gene Ontology (GO). For Fig 2B, Appendix Fig S7B and C only categories with FDR  $< 0.05$  were considered; while for Appendix Fig S6 only categories with FDR  $< 0.01$  were considered. David GO for the *Pum1* interactome in Fig 2B considered the entire interactome as background. For the GO regarding the HITS-CLIP targets shared among *Pum1*, *Pum2*, *Fmrp*, *Ago2*, and *Rbfox3* (Appendix Fig S7B and C), we considered the entire set of all targetomes together as background. Regarding the Synaptic (Syn) GO analysis (Appendix Fig S6), brain-expressed genes were used as background (Koopmans et al, 2019).

### Myc and GST cloning procedure with *in vitro* immunoprecipitation (IP) assays

Human *PUM1* full-length cDNA was amplified by PCR and subcloned in a pRK5 plasmid containing the Myc tag sequence (Addgene, pRK5-Myc-Parkin #17612) at the N-terminal by using *Sall* (New England Biolabs, # R3138S) and *NotI* (New England Biolabs, #R0189S) restriction enzymes to replace *Parkin* with *PUM1*. For GST, the human full-length *PUM1* cDNA was, again, subcloned first in the pRK5 plasmid containing the GST tag sequence (Addgene, pRK5-HA GST RagC wt, #19304) at the N-terminal by using *Sall* and *NotI* restriction enzymes to replace *RagC* with *PUM1*. Human *FMRP*, *AGO2* and *CNOT1*, full-length cDNA were cloned and contain the GST tag sequence at the N-terminal, as described for GST-*PUM1*.

To introduce the T1035S or R1147W mutations, we used the QuikChange II XL Multi Site-Directed Mutagenesis kit (Agilent Technologies, #200521). The primers for the single mutagenesis experiments were designed by QuikChange software (Stratagene, San Diego, <https://www.genomics.agilent.com/primerDesignProgram.jsp>).

For IP, HEK293T cells were seeded in 6-well plates for 24 h and then transfected with 250 ng of either WT or mutant *PUM1* plasmid with one of the interactors using the jetPRIME Transfection Reagent

(Polyplus transfection, #55-132) as per the manufacturer's protocol. pRK5-Myc empty plasmid (no cDNA) was used as a negative control. After 48 h, the cells were collected and processed for immunoprecipitation. Protein lysates were incubated overnight at 4°C with mouse  $\alpha$ -Myc antibody (1:400 [Cell Signaling Technologies, #2276]) on a rotisserie tube rotator. The next day, the beads were washed four times with an IP lysis buffer and resuspended in 40  $\mu$ l elution buffer (lysis buffer, NuPAGE 10 $\times$  Reducing Agent [Invitrogen, #NP0009], NuPAGE LDS sample buffer 4 $\times$  [Invitrogen, #NP0007]) and boiled at 95°C for 10 min before loading the samples in NuPAGE 4–12% Bis-Tris Gels (Invitrogen, #NP0335BOX & #NP0336BOX) for further resolution and western blot analysis. Antibodies: mouse  $\alpha$ -Myc antibody (1:2,000 [Cell Signaling Technologies, #2276]), rabbit  $\alpha$ -GST antibody (1:1,000 [Cell Signaling Technologies, #2625]), mouse  $\alpha$ -GAPDH (1:10,000 [Millipore, #CB1001]).

### Patient-derived cell lines

Primary fibroblasts from the *PUM1* PADDAS patient (9-year-old female) and the age- and sex-matched controls (three different 9-year-old female) were generated as previously described (Gennarino et al, 2018). Briefly, cells were isolated from skin biopsies taken from the patient or age-matched controls using standard methodology (Barch and Association of Cytogenetic Technology, 1991) and placed in a transport medium (Ham's F10, Thermo Scientific, #11550043). The skin specimen was later removed from the transport medium using a sterile technique (in a Class II biohazard cabinet) and transferred to a sterile Petri dish where it was cut into small pieces ( $< 0.5$  mm) using sterile scalpel blades. These pieces were transferred to the lower surface of a 25 cm<sup>2</sup> culture flask (6–8 pieces per flask), which had been pre-moistened with 1–2 ml of AmnioMAX Complete Medium (Thermo Scientific, #11269016) supplemented with 1% penicillin/streptomycin (GenDepot, #CA005-010). Cell cultures were maintained at 37°C in a humidified incubator supplemented with 5% CO<sub>2</sub>. When cell growth was observed around the edges of the tissue, usually 3–5 days later, 2–3 ml of AmnioMAX Complete Medium was added. Once growth was established and the tissue was anchored to the flask, another 8 ml of AmnioMAX Complete Medium was added. Thereafter, the medium was renewed every 3–4 days until ready for sub-culturing.

Lymphoblastoid cells from *PUM1* PRCA patients (female 59 and 58 years old, respectively) and the age- and sex-matched controls (three different 58-year-old female) were generated as previously described (Gennarino et al, 2018). Briefly, lymphoblastoid suspension cell cultures were grown in RPMI 1640 medium (Invitrogen, #11875093) supplemented with 10% heat-inactivated fetal bovine serum (Atlanta Biological, Flowery Branch, #S11195H) and 1% penicillin/streptomycin (GenDepot, #CA005-010). Cell cultures were maintained at 37°C in a humidified incubator supplemented with 5% CO<sub>2</sub>. Medium was renewed every 2–3 days.

### Fibroblast patient-derived cell lines transfection

Fibroblasts from age- and sex-matched healthy controls and from a female PADDAS patient were seeded at 80% of confluency in 6-well plates ( $\sim 150,000$  cells/well). The day after, 500 ng of pRK5-CMV-Myc-Pum1 or pRK5-CMV-Myc-Empty plasmids was transfected in antibiotic-free DMEM (GenDepot, #CM002-320) using Lipofectamine

LTX with Plus Reagent (Thermo Fisher, #15338030) according to the manufacturer's protocol. After 5 h we replaced the media with new complete DMEM supplemented with 10% of heat-inactivated fetal bovine serum (FBS [GenDepot, #F0901-050]) and 1% penicillin/streptomycin (GenDepot, #CA005-010). Cells were incubated at 37°C in a humidified chamber supplemented with 5% CO<sub>2</sub> and collected after 72 h for RNA and protein extraction.

### Primers

For the qPCR analysis to unambiguously distinguish spliced cDNA from genomic DNA contamination, specific exon primers were designed to amplify across introns of the gene tested. The primers for all genes tested were designed with Primer3 (Koressaar & Remm, 2007; Untergasser *et al.*, 2012). Cloning primers were manually designed to amplify the longest spliced gene isoform tested; if there was more than one isoform according to the UCSC Genome Browser (<https://genome.ucsc.edu/>), we chose the longest. See Dataset EV7 for primer sequences.

### Ethical statement and mouse strains

All animal procedures were approved by the Institutional Animal Care and Use Committee at Columbia University, New York under the protocol AC-AAAU8490. Mice were maintained on a 12-h light, 12-h dark cycle with regular chow and water *ad libitum*. Puml knockout mice were generated as previously described (Chen *et al.*, 2012). C57BL/6J wild-type mice were purchased from Jackson Laboratory and maintained as described above. For brain dissection, mice were anesthetized with isoflurane, and the brain rapidly removed from the skull and lysed in the appropriate buffer according to the experiment (see [Materials and Methods](#) details).

### Experimental design

For protein and RNA quantification from patient-derived cell lines, we used values from at least six independent experiments with three biological replicates for each experiment. At every stage of the study, the experimenter was blinded to the identity of control and patient-derived cell lines. For example, for the data regarding both human patient-derived cell lines and mice, Experimenter #1 made a list of samples and controls to be tested, and Experimenter #2 randomized this list and relabeled the tubes; Experimenter #2 was the only person with the key to identify the samples. These samples were then distributed to Experimenter #3 to culture the cells, then to Experimenter #1 to perform western blots and qRT-PCR, and lastly Experimenters #1 and #4 analyzed the data. Only then was the key applied to identify the samples.

For mouse experiments, the experimenters were randomized and blinded as described above. The number of animals used and sex and the specific statistical tests used are indicated for each experiment in the figure legends. Sample size was based on previous experience using the same mice (Gennarino *et al.*, 2015).

### Software and statistical analysis

Statistical significance was analyzed using GraphPad Prism 8 (<https://www.graphpad.com/scientific-software/prism/>) and Excel

(Microsoft). All data are presented as mean  $\pm$  SEM. Statistical details for each experiment can be found in the figures and the legends. The range of expression levels in qPCR was determined from at least six independent experiments with three biological replicates by calculating the standard deviation of the  $\Delta C_t$  (Pfaffl, 2001). The range of expression levels in western blots was determined from at least six independent experiments with at least six biological replicates. *P* values were calculated by Student's *T*-test or analysis of variance with Tukey's *post hoc* analysis. For the IP in Fig 6A and protein quantification in patient cell lines in Fig 6C, we had only one PADDAS patient, so the repeated experiments were technical replicates rather than biological replicates. We therefore calculated the statistical significance based on these technical replicates in comparison to the three biological replicates (i.e., healthy controls).

### Study approval

PADDAS and PRCA patient cell lines are the same as those reported previously (Gennarino *et al.*, 2018). The consent form for each subject specifically allows for sharing of medical information and physical exam findings; the sharing of cell lines from the PADDAS and PRCA subjects and the controls was approved under the Columbia University Medical Center IRB-AAAS7401 (Y01M00) and the Baylor College of Medicine IRB H-34578.

## Data availability

IP mass spec and quantitative proteomics raw data are available at <https://massive.ucsd.edu/ProteoSAFe/static/massive.jsp?redirect=auth> with accession number MSV000089941. microRNA sequencing raw data are available at <https://www.ncbi.nlm.nih.gov/geo/query/acc.cgi> using the GEO number GSE207031. All source data related to this manuscript are available at BioStudies: <https://www.ebi.ac.uk/biostudies/> accession number S-BSST1046.

**Expanded View** for this article is available [online](#).

### Acknowledgments

We thank the patients and their families for participating in our study. We thank Mingyu Cao for help with statistical analyses, U.N. Wasko for starting the cloning procedure with Myc and GST tag sequences *in vitro*, W. Miles for sharing the RIP protocol and the HCT116-*PUM1*<sup>-/-</sup> cell lines, and J. T. Mendell for providing the MBP-SNAP-PUM1-His<sub>6</sub>. We thank V. Ambros and G. Struhl for encouragement early in the project, H.Y. Zoghbi and G. Karsenty for comments on an early draft, and Y. Giardina and members of the Gennarino lab for helpful discussions and support. This work was supported by the National Institute of Neurological Disorders and Stroke (NINDS; R01NS109858 to V.A.G.); the National Ataxia Foundation/Young Investigator Research Grant (V.A.G.); the National Institute of General Medical Sciences (NIGMS; R35GM128855 to N.G.B.); the National Human Genome Research Institute (NHGRI; R01HG012216 to M.J.); the National Institute on Aging (NIA; R01AG071869 to M.J.); the National Institute of General Medicine (NIGM; R35GM128802 to M.J.); the Brain & Behavior Research Foundation Young Investigator Award (V.A.G.); the Paul A. Marks Scholar Program, Columbia University Vagelos College of Physicians and Surgeons (V.A.G.); the TIGER Award, Taub Institute, Columbia University Irving Medical Center (V.A.G.); the Columbia Stem Cell Initiative (CSCI), Columbia University Irving Medical Center (V.A.G. and N.d.P.). The authors declare no competing interests.

## Author contributions

**Salvatore Botta:** Formal analysis; validation; investigation; visualization; methodology; writing – original draft. **Nicola de Prisco:** Formal analysis; validation; investigation; visualization; writing – review and editing. **Alexei Chemiakine:** Formal analysis; validation; investigation; methodology. **Vicky Brandt:** Formal analysis; writing – original draft; writing – review and editing. **Maximilian Cabaj:** Validation; investigation; writing – original draft. **Purvi Patel:** Resources; data curation; formal analysis. **Ella Doron-Mandel:** Resources; data curation; formal analysis. **Colton J Treadway:** Formal analysis; investigation; methodology. **Marko Jovanovic:** Resources; data curation; writing – review and editing. **Nicholas G Brown:** Data curation; methodology; writing – review and editing. **Rajesh K Soni:** Resources; data curation; methodology. **Vincenzo A Gennarino:** Conceptualization; resources; data curation; formal analysis; supervision; funding acquisition; validation; investigation; visualization; methodology; writing – original draft; project administration; writing – review and editing.

## Disclosure and competing interests statement

The authors declare that they have no conflict of interest.

## References

- Agarwal V, Bell GW, Nam JW, Bartel DP (2015) Predicting effective microRNA target sites in mammalian mRNAs. *Elife* 4: e05005
- Blackinton JG, Keene JD (2014) Post-transcriptional RNA regulons affecting cell cycle and proliferation. *Semin Cell Dev Biol* 34: 44–54
- Blewett NH, Goldstrohm AC (2012) A eukaryotic translation initiation factor 4E-binding protein promotes mRNA decapping and is required for PUF repression. *Mol Cell Biol* 32: 4181–4194
- Charizanis K, Lee KY, Batra R, Goodwin M, Zhang C, Yuan Y, Shiue L, Cline M, Scotti MM, Xia G et al (2012) Muscleblind-like 2-mediated alternative splicing in the developing brain and dysregulation in myotonic dystrophy. *Neuron* 75: 437–450
- Chartier-Harlin MC, Kachergus J, Roumier C, Mouroux V, Douay X, Lincoln S, Levecque C, Larvor L, Andrieux J, Hulihan M et al (2004) Alpha-synuclein locus duplication as a cause of familial Parkinson's disease. *Lancet* 364: 1167–1169
- Chen D, Zheng W, Lin A, Uyhazi K, Zhao H, Lin H (2012) Pumilio 1 suppresses multiple activators of p53 to safeguard spermatogenesis. *Curr Biol* 22: 420–425
- Chi SW, Zang JB, Mele A, Darnell RB (2009) Argonaute HITS-CLIP decodes microRNA-mRNA interaction maps. *Nature* 460: 479–486
- Coffin SL, Durham MA, Nitschke L, Xhako E, Brown AM, Revelli JP, Villavicencio Gonzalez E, Lin T, Handler HP, Dai Y et al (2022) Disruption of the ATXN1-CIC complex reveals the role of additional nuclear ATXN1 interactors in spinocerebellar ataxia type 1. *Neuron* 111: 915
- Conboy JG (2017) Developmental regulation of RNA processing by Rbfox proteins. *Wiley Interdiscip Rev RNA* 8: <https://doi.org/10.1002/wrna.1398>
- Cox J, Mann M (2008) MaxQuant enables high peptide identification rates, individualized p.p.b.-range mass accuracies and proteome-wide protein quantification. *Nat Biotechnol* 26: 1367–1372
- Cox J, Neuhauser N, Michalski A, Scheltema RA, Olsen JV, Mann M (2011) Andromeda: a peptide search engine integrated into the MaxQuant environment. *J Proteome Res* 10: 1794–1805
- Darnell JC, Richter JD (2012) Cytoplasmic RNA-binding proteins and the control of complex brain function. *Cold Spring Harb Perspect Biol* 4: a012344
- Dassi E (2017) Handshakes and fights: the regulatory interplay of RNA-binding proteins. *Front Mol Biosci* 4: 67
- De Maio A, Yalamanchili HK, Adamski CJ, Gennarino VA, Liu Z, Qin J, Jung SY, Richman R, Orr H, Zoghbi HY (2018) RBM17 interacts with U2SURP and CHERP to regulate expression and splicing of RNA-processing proteins. *Cell Rep* 25: 726–736.e7
- Di Grazia A, Marafini I, Pedini G, Di Fusco D, Laudisi F, Dinallo V, Rosina E, Stolfi C, Franze E, Sileri P et al (2021) The fragile X mental retardation protein regulates RIPK1 and colorectal cancer resistance to necroptosis. *Cell Mol Gastroenterol Hepatol* 11: 639–658
- Elguindy MM, Mendell JT (2021) NORAD-induced Pumilio phase separation is required for genome stability. *Nature* 595: 303–308
- Enwerem III, Elrod ND, Chang CT, Lin A, Ji P, Bohn JA, Levdansky Y, Wagner EJ, Valkov E, Goldstrohm AC (2021) Human Pumilio proteins directly bind the CCR4-NOT deadenylase complex to regulate the transcriptome. *RNA* 27: 445–464
- Friend K, Campbell ZT, Cooke A, Kroll-Conner P, Wickens MP, Kimble J (2012) A conserved PUF-ago-eEF1A complex attenuates translation elongation. *Nat Struct Mol Biol* 19: 176–183
- Fu J, Peng L, Tao T, Chen Y, Li Z, Li J (2019) Regulatory roles of the miR-200 family in neurodegenerative diseases. *Biomed Pharmacother* 119: 109409
- Gennarino VA, D'Angelo G, Dharmalingam G, Fernandez S, Russolillo G, Sanges R, Mutarelli M, Belcastro V, Ballabio A, Verde P et al (2012) Identification of microRNA-regulated gene networks by expression analysis of target genes. *Genome Res* 22: 1163–1172
- Gennarino VA, Singh RK, White JJ, De Maio A, Han K, Kim JY, Jafar-Nejad P, di Ronza A, Kang H, Sayegh LS et al (2015) Pumilio1 haploinsufficiency leads to SCA1-like neurodegeneration by increasing wild-type Ataxin1 levels. *Cell* 160: 1087–1098
- Gennarino VA, Palmer EE, McDonell LM, Wang L, Adamski CJ, Koire A, See L, Chen CA, Schaaf CP, Rosenfeld JA et al (2018) A mild PUM1 mutation is associated with adult-onset ataxia, whereas haploinsufficiency causes developmental delay and seizures. *Cell* 172: 924–936.e11
- Giurgiu M, Reinhard J, Brauner B, Dunger-Kaltenbach I, Fobo G, Frishman G, Montrone C, Ruepp A (2019) CORUM: the comprehensive resource of mammalian protein complexes-2019. *Nucleic Acids Res* 47: D559–D563
- Goldstrohm AC, Hall TMT, McKenney KM (2018) Post-transcriptional regulatory functions of mammalian Pumilio proteins. *Trends Genet* 34: 972–990
- Hentze MW, Castello A, Schwarzl T, Preiss T (2018) A brave new world of RNA-binding proteins. *Nat Rev Mol Cell Biol* 19: 327–341
- Huh SU (2021) The role of Pumilio RNA binding protein in plants. *Biomolecules* 11: 1851
- Kedde M, van Kouwenhove M, Zwart W, Oude Vrielink JA, Elkon R, Agami R (2010) A Pumilio-induced RNA structure switch in p27-3' UTR controls miR-221 and miR-222 accessibility. *Nat Cell Biol* 12: 1014–1020
- Keene JD (2007a) Biological clocks and the coordination theory of RNA operons and regulons. *Cold Spring Harb Symp Quant Biol* 72: 157–165
- Keene JD (2007b) RNA regulons: coordination of post-transcriptional events. *Nat Rev Genet* 8: 533–543
- Keene JD, Lager PJ (2005) Post-transcriptional operons and regulons coordinating gene expression. *Chromosome Res* 13: 327–337
- Kenny PJ, Zhou H, Kim M, Skariah G, Khetani RS, Drnevich J, Arcila ML, Kosik KS, Ceman S (2014) MOV10 and FMRP regulate AGO2 association with microRNA recognition elements. *Cell Rep* 9: 1729–1741
- Kenny PJ, Kim M, Skariah G, Nielsen J, Lannom MC, Ceman S (2020) The FMRP-MOV10 complex: a translational regulatory switch modulated by G-quadruplexes. *Nucleic Acids Res* 48: 862–878

- Khalil B, Morderer D, Price PL, Liu F, Rossoll W (2018) mRNP assembly, axonal transport, and local translation in neurodegenerative diseases. *Brain Res* 1693: 75–91
- Kim K, Hessel D, Randol JL, Espinal GM, Schneider A, Protic D, Aydin EY, Hagerman RJ, Hagerman PJ (2019) Association between IQ and FMR1 protein (FMRP) across the spectrum of CGG repeat expansions. *PLoS One* 14: e0226811
- Koopmans F, van Nierop P, Andres-Alonso M, Byrnes A, Cijssouw T, Coba MP, Cornelisse LN, Farrell RJ, Goldschmidt HL, Howrigan DP et al (2019) SynGO: an evidence-based, expert-curated Knowledge Base for the synapse. *Neuron* 103: 217–234.e4
- Koressaar T, Remm M (2007) Enhancements and modifications of primer design program Primer3. *Bioinformatics* 23: 1289–1291
- Lee Y, Samaco RC, Gatchel JR, Thaller C, Orr HT, Zoghbi HY (2008) miR-19, miR-101 and miR-130 co-regulate ATXN1 levels to potentially modulate SCA1 pathogenesis. *Nat Neurosci* 11: 1137–1139
- Lee S, Kopp F, Chang TC, Sataluri A, Chen B, Sivakumar S, Yu H, Xie Y, Mendell JT (2016) Noncoding RNA NORAD regulates genomic stability by sequestering PUMILIO proteins. *Cell* 164: 69–80
- Lee EJ, Seo E, Kim JW, Nam SA, Lee JY, Jun J, Oh S, Park M, Jho EH, Yoo KH et al (2020) TAZ/Wnt-beta-catenin/c-MYC axis regulates cystogenesis in polycystic kidney disease. *Proc Natl Acad Sci USA* 117: 29001–29012
- Licatalosi DD, Yano M, Fak JJ, Mele A, Grabinski SE, Zhang C, Darnell RB (2012) Ptbp2 represses adult-specific splicing to regulate the generation of neuronal precursors in the embryonic brain. *Genes Dev* 26: 1626–1642
- Lin K, Qiang W, Zhu M, Ding Y, Shi Q, Chen X, Zsiros E, Wang K, Yang X, Kurita T et al (2019) Mammalian Pum1 and Pum2 control body size via translational regulation of the cell cycle inhibitor Cdkn1b. *Cell Rep* 26: 2434–2450.e6
- Marrero E, Rossi SG, Darr A, Tsoulfas P, Rotundo RL (2011) Translational regulation of acetylcholinesterase by the RNA-binding protein Pumilio-2 at the neuromuscular synapse. *J Biol Chem* 286: 36492–36499
- Mauger O, Lemoine F, Scheiffele P (2016) Targeted intron retention and excision for rapid gene regulation in response to neuronal activity. *Neuron* 92: 1266–1278
- Maurin T, Lebrigand K, Castagnola S, Paquet A, Jarjat M, Popa A, Grossi M, Rage F, Bardoni B (2018) HITS-CLIP in various brain areas reveals new targets and new modalities of RNA binding by fragile X mental retardation protein. *Nucleic Acids Res* 46: 6344–6355
- Miles WO, Tschop K, Herr A, Ji JY, Dyson NJ (2012) Pumilio facilitates miRNA regulation of the E2F3 oncogene. *Genes Dev* 26: 356–368
- Muraro NI, Weston AJ, Gerber AP, Luschnig S, Moffat KG, Baines RA (2008) Pumilio binds Para mRNA and requires Nanos and brat to regulate sodium current in drosophila motoneurons. *J Neurosci* 28: 2099–2109
- Otasek D, Morris JH, Boucas J, Pico AR, Demchak B (2019) Cytoscape automation: empowering workflow-based network analysis. *Genome Biol* 20: 185
- Pfaffl MW (2001) A new mathematical model for relative quantification in real-time RT-PCR. *Nucleic Acids Res* 29: e45
- Preitner N, Quan J, Nowakowski DW, Hancock ML, Shi J, Tcherkezian J, Young-Pearse TL, Flanagan JG (2014) APC is an RNA-binding protein, and its interactome provides a link to neural development and microtubule assembly. *Cell* 158: 368–382
- Rappilber J, Mann M, Ishihama Y (2007) Protocol for micro-purification, enrichment, pre-fractionation and storage of peptides for proteomics using StageTips. *Nat Protoc* 2: 1896–1906
- Raudvere U, Kolberg L, Kuzmin I, Arak T, Adler P, Peterson H, Vilo J (2019) G: profiler: a web server for functional enrichment analysis and conversions of gene lists (2019 update). *Nucleic Acids Res* 47: W191–W198
- Ravanidis S, Kattan FG, Doxakis E (2018) Unraveling the pathways to neuronal homeostasis and disease: mechanistic insights into the role of RNA-binding proteins and associated factors. *Int J Mol Sci* 19: 2280
- Rousseaux MWC, Tschumperlin T, Lu HC, Lackey EP, Bondar VV, Wan YW, Tan Q, Adamski CJ, Friedrich J, Twaroski K et al (2018) ATXN1-CIC complex is the primary driver of cerebellar pathology in spinocerebellar ataxia type 1 through a gain-of-function mechanism. *Neuron* 97: 1235–1243.e5
- Rovelet-Lecrux A, Hannequin D, Raux G, Le Meur N, Laquerriere A, Vital A, Dumanchin C, Feuillette S, Brice A, Vercelletto M et al (2006) APP locus duplication causes autosomal dominant early-onset Alzheimer disease with cerebral amyloid angiopathy. *Nat Genet* 38: 24–26
- Shah S, Molinaro G, Liu B, Wang R, Huber KM, Richter JD (2020) FMRP control of ribosome translocation promotes chromatin modifications and alternative splicing of neuronal genes linked to autism. *Cell Rep* 30: 4459–4472.e6
- Shannon P, Markiel A, Ozier O, Baliga NS, Wang JT, Ramage D, Amin N, Schwikowski B, Ideker T (2003) Cytoscape: a software environment for integrated models of biomolecular interaction networks. *Genome Res* 13: 2498–2504
- Shevchenko A, Tomas H, Havlis J, Olsen JV, Mann M (2006) In-gel digestion for mass spectrometric characterization of proteins and proteomes. *Nat Protoc* 1: 2856–2860
- Singh K, Prasad S (2008) Differential expression of Fmr-1 mRNA and FMRP in female mice brain during aging. *Mol Biol Rep* 35: 677–684
- Singh K, Gaur P, Prasad S (2007) Fragile x mental retardation (Fmr-1) gene expression is down regulated in brain of mice during aging. *Mol Biol Rep* 34: 173–181
- Smidak R, Sialana FJ, Kristofova M, Stojanovic T, Rajcic D, Malikovic J, Feyissa DD, Korz V, Hoeger H, Wackerlig J et al (2017) Reduced levels of the synaptic functional regulator FMRP in dentate gyrus of the aging Sprague-Dawley rat. *Front Aging Neurosci* 9: 384
- Sternburg EL, Estep JA, Nguyen DK, Li Y, Karginov FV (2018) Antagonistic and cooperative AGO2-PUM interactions in regulating mRNAs. *Sci Rep* 8: 15316
- Subramanian A, Tamayo P, Mootha VK, Mukherjee S, Ebert BL, Gillette MA, Paulovich A, Pomeroy SL, Golub TR, Lander ES et al (2005) Gene set enrichment analysis: a knowledge-based approach for interpreting genome-wide expression profiles. *Proc Natl Acad Sci USA* 102: 15545–15550
- Takeguchi R, Takahashi S, Kuroda M, Tanaka R, Suzuki N, Tomonoh Y, Ihara Y, Sugiyama N, Itoh M (2020) MeCP2\_e2 partially compensates for lack of MeCP2\_e1: a male case of Rett syndrome. *Mol Genet Genomic Med* 8: e1088
- Temme C, Simonelig M, Wahle E (2014) Deadenylation of mRNA by the CCR4-NOT complex in drosophila: molecular and developmental aspects. *Front Genet* 5: 143
- Thul PJ, Akesson L, Wiking M, Mahdessian D, Geladaki A, Ait Blal H, Alm T, Asplund A, Bjork L, Breckels LM et al (2017) A subcellular map of the human proteome. *Science* 356: eaal3321
- Trumbach D, Prakash N (2015) The conserved miR-8/miR-200 microRNA family and their role in invertebrate and vertebrate neurogenesis. *Cell Tissue Res* 359: 161–177
- Tyanova S, Temu T, Sinitcyn P, Carlson A, Hein MY, Geiger T, Mann M, Cox J (2016) The Perseus computational platform for comprehensive analysis of (prote)omics data. *Nat Methods* 13: 731–740



- Untergasser A, Cutcutache I, Koressaar T, Ye J, Faircloth BC, Remm M, Rozen SG (2012) Primer3—new capabilities and interfaces. *Nucleic Acids Res* 40: e115
- Uyhazi KE, Yang Y, Liu N, Qi H, Huang XA, Mak W, Weatherbee SD, de Prisco N, Gennarino VA, Song X et al (2020) Pumilio proteins utilize distinct regulatory mechanisms to achieve complementary functions required for pluripotency and embryogenesis. *Proc Natl Acad Sci USA* 117: 7851–7862
- Van Etten J, Schagat TL, Hrit J, Weidmann CA, Brumbaugh J, Coon JJ, Goldstrohm AC (2012) Human Pumilio proteins recruit multiple deadenylases to efficiently repress messenger RNAs. *J Biol Chem* 287: 36370–36383
- Vandesompele J, De Preter K, Pattyn F, Poppe B, Van Roy N, De Paepe A, Speleman F (2002) Accurate normalization of real-time quantitative RT-PCR data by geometric averaging of multiple internal control genes. *Genome Biol* 3: research0034
- Wamsley B, Jaglin XH, Favuzzi E, Quattrocchio G, Nigro MJ, Yusuf N, Khodadadi-Jamayran A, Rudy B, Fishell G (2018) Rbfox1 mediates cell-type-specific splicing in cortical interneurons. *Neuron* 100: 846–859.e7
- Weidmann CA, Raynard NA, Blewett NH, Van Etten J, Goldstrohm AC (2014) The RNA binding domain of Pumilio antagonizes poly-adenosine binding protein and accelerates deadenylation. *RNA* 20: 1298–1319
- Weyn-Vanhenryck SM, Mele A, Yan Q, Sun S, Farny N, Zhang Z, Xue C, Herre M, Silver PA, Zhang MQ et al (2014) HITS-CLIP and integrative modeling define the Rbfox splicing-regulatory network linked to brain development and autism. *Cell Rep* 6: 1139–1152
- Wickens M, Bernstein DS, Kimble J, Parker R (2002) A PUF family portrait: 3'UTR regulation as a way of life. *Trends Genet* 18: 150–157
- Zamore PD, Williamson JR, Lehmann R (1997) The Pumilio protein binds RNA through a conserved domain that defines a new class of RNA-binding proteins. *RNA* 3: 1421–1433
- Zhang C, Frias MA, Mele A, Ruggiu M, Eom T, Marney CB, Wang H, Licatalosi DD, Fak JJ, Darnell RB (2010) Integrative modeling defines the Nova splicing-regulatory network and its combinatorial controls. *Science* 329: 439–443
- Zhang M, Chen D, Xia J, Han W, Cui X, Neuenkirchen N, Hermes G, Sestan N, Lin H (2017) Post-transcriptional regulation of mouse neurogenesis by Pumilio proteins. *Genes Dev* 31: 1354–1369



**License:** This is an open access article under the terms of the [Creative Commons Attribution](#) License, which permits use, distribution and reproduction in any medium, provided the original work is properly cited.